NASA/TM—1998-207916

Dynamics of Liquids in Edges and Corners (DYLCO) IML–2 Experiment for the BDPU

D. Langbein
ZARM, University of Bremen, Germany

M. Weislogel
Lewis Research Center, Cleveland, Ohio

National Aeronautics and
Space Administration

Lewis Research Center

August 1998

Acknowledgments

We would like to thank Payload Specialist, Chiaki Mukai, who spent extra time on our experiment; the ground Support Team of ESTEC, in particular, Pasquale DiPalermo, and the ground support teams of Dornier and Mars.

This work has been supported by the Deutsche Agentur fur Raumfahrtangelegenheiten, DARA, under contract number 50 WM 9432.

Available from

NASA Center for Aerospace Information
7121 Standard Drive
Hanover, MD 21076
Price Code: A03

National Technical Information Service
5287 Port Royal Road
Springfield, VA 22100
Price Code: A03

DYNAMICS OF LIQUIDS IN EDGES AND CORNERS (DYLCO) -IML-2 EXPERIMENT FOR THE BDPU-

D. Langbein
ZARM, University of Bremen
Germany

and

M. Weislogel
National Aeronautics and Space Administration
Lewis Research Center
Cleveland, Ohio 44135

SUMMARY

Knowledge of the behavior of fluids possessing free surfaces is important to many fluid systems, particularly in space, where the normally subtle effects of surface wettability play a more dramatic and often surprising role. DYLCO for the IML-2 mission was proposed as a simple experiment to probe the particular behavior of capillary surfaces in containers of irregular cross section. Temperature control was utilized to vary the fluid-solid contact angle, a questionable thermodynamic parameter of the system, small changes in which can dramatically influence the configuration, stability, and flow of a capillary surface. Container shapes, test fluid, and temperature ranges were selected for observing both local changes in interface curvature as well as a global change in fluid orientation due to a critical wetting phenomenon. The experiment hardware performed beyond what was expected and fluid interfaces could be readily digitized post flight to show the dependence of the interface curvature on temperature. For each of the containers tested surfaces were observed which did not satisfy the classic equations for the prediction of interface shape with constant contact angle boundary condition. This is explained by the presence of contact angle hysteresis arising from expansion and contraction of the liquid during the heating and cooling steps of the test procedure. More importantly, surfaces exceeding the critical surface curvature required for critical wetting were measured, yet no wetting was observed. These findings are indeed curious and pose key questions concerning the role of hysteresis for this critical wetting phenomena. The stability of such surfaces was determined numerically and it is shown that stability is enhance (reduced) when a surface is in its 'advancing' ('receding') state. The analysis shows complete instability as the critical wetting condition is reached. The case of ideal dynamic wetting is addressed analytically in detail with results of significant flow characteristics presented in closed form. The solutions indicate a $\sqrt{t}$ dependence of the capillary 'rise' rate which is corroborated by drop tower tests. The analysis clearly shows that infinite time is necessary for surfaces to reorient at the critical wetting transition.

1. OBJECTIVE

As part of a larger study to investigate the overall characteristics of the static and dynamic behavior of capillary surfaces, the Dynamics of Liquids in Edges and Corners experiment (DYLCO) for the 2nd International Microgravity Laboratory shuttle flight STS-65 (IML-2) was proposed as a simple experiment to probe the particular behavior of capillary surfaces in containers of rhombic cross section. The objective was to utilize temperature control to vary the fluid-solid contact angle, γ, a questionable thermodynamic parameter of the system, small changes in which can dramatically influence the configuration, stability, and flow of a capillary surface.

The onboard filling of four slightly differing test cells and the resulting fluid interface shapes were recorded using a 16 mm cine camera. A refractive index matched transparent cell material and test fluid were used to minimize optical distortions and allow the interface shapes to be digitized directly from the film records post flight. These data served as our quantitative measurements for our accompanying analyses.

Our principal interest was to measure changes in static interface shapes with changes in system temperature. (The original intention of studying the influence of electrocapillarity had to be canceled due to the

safety requirements of the Space Shuttle. Changing the surface tension and the contact angle by changing the temperature was chosen instead.) From a thermodynamic point of view the contact angle (angle of contact of the liquid-gas interface and a solid boundary measured in the liquid phase) is known and expected to decrease with increasing temperature until complete wetting is established [Cahn (1977)]. As has been clearly shown [Concus and Finn (1990)] for the case of low-gravity, the surface shape of a fluid interface, or interface configuration, is dictated almost entirely by the container shape and fluid/solid contact angle. The ability to change the contact angle in a system where all else is fixed provides a unique ability to note the variety of surfaces which can form in a single vessel due to contact angle. Not only are changes in local shape anticipated, but gross reorientation of the fluid is possible in some cases. The intention of DYLCO was to observe both local and global shifts in the fluid orientation due to small changes in the contact angle. Information regarding such, in addition to being of interest to the theoretician, is key to the design of fluid systems in space.

2. BACKGROUND

In the zero gravity environment, the configuration of a fluid interface is dictated solely by the container shape and the fluid-solid contact angle. Thus by a judicious selection of each one might be able to control, in a passive manner, the location of the bulk fluid. Such information is valuable for in-space fluid separation processes, liquid fuel/oxygen storage and transport, fluid waste management, passive thermal systems such as heat pipes, and fluids and materials microgravity experiment design.

DYLCO was aimed at confirming the existence and the stability limits of selected liquid surfaces in right cylinders of rhombic cross section. For a fixed fluid volume and test cell, a change of the contact angle (γ) between 0 and π can produce three entirely different global surface configurations. These will be outlined below for a vessel of fixed principal vertex half angle α. The 'principal vertex' of the rhombus is taken to be the interior corners with the smallest dihedral angle. Figure 1 illustrates several possibilities.

Case I. $\gamma \leq \pi/2 - \alpha$: (critical wetting-liquid phase).—When the contact angle satisfies this condition a capillary underpressure is established in the liquid which acts to further draw the liquid into the corner. Curvature of the surface in the plane perpendicular to the corner axis dominates the flow and the eventual surface configuration is dependent of the specific values of α and γ and the fluid volume. Mathematically, in the limit of zero gravity, the fluid would climb to an infinite extent. Changes of the contact angle within this domain effect relatively local changes in surface configuration as well as the rate of flow/reorientation. It is not difficult to appreciate the value of the ability to predict, and hence control, such flows. Many currently existing space fluids systems that rely on the passive positioning of liquids in partially filled tanks exploit this phenomena; a prime example being Propellant Management Devices (PMD s) commonly resident in satellite fuel tanks [Rollins, et al. (1986)].

Case II. $\pi/2 - \alpha < \gamma < \pi/2 + \alpha$: (portion of spherical surface).—When the contact angle satisfies this condition curvature in planes parallel and perpendicular to the corner axis play an equal role and surfaces result which in general cover the base of the cell and are portions of a sphere. Figure 1 provides one illustrative example. Transitions between Case I and Case II can lead to break up of the slender fluid columns in the corners in the same manner as a free cylindrical jet becomes unstable if its length exceeds its circumference [Langbein (1990)]. Such surfaces are common in containers of simple geometry like the right circular cylinder.

Case III. $\gamma \geq \pi/2 + \alpha$: (critical wetting-gas phase).—This condition results in the identical behavior of Case I only the fluid phases are reversed—the liquid is contained in the central core of the test cell while the gas phase wets the corners and at least a portion if not all of the base(s).

3. METHOD OF DATA ACQUISITION/ANALYSIS

Cases I and II were studied in this work. Ground based experiments performed in drop towers in both Bremen and Cleveland were performed to investigate the more dynamic fluid phenomena associated with Case I while DYLCO provided quantitative results primarily concerning Case II where forces are significantly smaller requiring extended low gravity time not afforded by current ground based facilities.

3.1 Flight and Drop Tower Experiments

3.1.1 DYLCO for the BDPU.—Four cylindrical vessels of rhombic cross section were fabricated out of fused silica (quartz) for the test. Figure 2 provides the cells with associated cross sections and the DYLCO apparatus.

The cells were made as large as the BDPU (Bubble, Drop, and Particle Unit) would allow. This was to minimize the effects of surface roughness, contamination, etc. on the anticipated motion of the free surface. The test fluid was a fused silica index of refraction matched liquid (code 50350) provided by Cargille Laboratories. The relevant temperature dependent properties of the fluid were measured and are presented in table I.

The interior surfaces of the test cells were coated with FC-724, a surface modifier supplied by the 3M Corporation. The coating was used to establish the desired wetting conditions in the cells. The uncoated cells show a contact angle of approximately 19° with the liquid used.

The BDPU itself is a multi-user facility designed for a variety of fluid physics experiments. Of the many diagnostic capabilities provided by the BDPU, DYLCO required power for heating and fluid transfer, background illumination, temperature measurement, cine camera photography and commanding. The DYLCO module was built as an interchangeable test container which could be inserted into the core of the BDPU. The DYLCO module was complete with rhombic test cells, onboard fluid reservoirs and fill apparatus for the charging of the test cells, and resistance heaters and temperature probes for thermal control.

During the flight the cells were partially filled via four independent fill ports. The temperature was then cycled from 20 to 80 °C in increments of 20 °C which required approximately 20 to 30 min/incremental increase. Though the originally planned peak temperature was 80 °C, the system temperature was further increased to 95 °C. The cooling steps followed similarly with the surface shapes being recorded on cine film after each step. Sample photographs of the fluid interfaces during the fill and thermal cycling are provided as figure 3. The change in curvature of the interface from the initial ambient condition (fig. 3(b) ambient) to the final ambient condition (fig. 3(c) ambient) is most easily observed and is attributable to the effects of contact angle hysteresis to be discussed shortly. Even in reprint the interfaces can be clearly distinguished leaving no need for post flight image enhancement.

The BDPU and DYLCO operated perfectly from the fill, to the photography, to the temperature commanding and control. As stated, it was actually possible to increase the temperature beyond what was originally planned without hazard. The freedom of complete commanding from the ground made for the relaxed and enjoyable conduct of the experiment. The high quality images from the cine films could readily be digitized for use in the post flight analysis.

3.1.2 DYLCO for the Drop Towers.—Functional tests of the flight apparatus were conducted in the Bremen drop tower and also in parabolic flights in Europe. In addition, research specific tests could be conducted in the drop tower for the condition of Case I outlined above since in cases of favorable wetting flow rates/reorientation rates are rapid enough that sufficient observation may be made in the limited drop time available. Drop tower tests at ZARM, in Bremen and at NASA Lewis Research Center in Cleveland were conducted along these lines with the flight cells and with other similar cells. A large amount of data was accumulated on fluid rise rates, volumetric flow rates, and surface profiles for comparison with the accompanying analyses for this problem. The tests themselves simply required the step reduction of gravity (common in drop towers) for a vessel partially filled with the test fluid. The resulting flows were captured on high speed cine camera film for subsequent data collection. Observation of the film records provided insight into the development of the theory which can now be shown to well represent the capillary driven corner flow that results when $\gamma \leq \pi/2 - \alpha$. The effects of corner angle and contact angle can also be confirmed which reveal clearly the decay of the corner flow velocity to zero as γ approaches $\pi/2 - \alpha$. As pointed out above, no corner flow takes place when $\pi/2 - \alpha < \gamma < \pi/2 + \alpha$, Case II.

A photographic sequence of sample data using the flight cells in the drop tower at ZARM is provided as figure 4 where the cells are left uncoated such that $\gamma \leq \pi/2 - \alpha$. The rise of the fluid in the corner can be seen by tracking the tip of a 'sword-like' dark region along the center line (principal dihedral angle axis) of the cell. Figure 5 displays the digitized tip location data for all four cells for a variety of system temperatures. Two important observations can be made from these results: The rise rate increases with increasing temperature and the rise rate is proportional to $\sqrt{t}$. This latter observation, displayed in figure. 6, will be exploited in the analysis to follow.

3.2 Analysis

Analyses were performed for Cases I and II outlined above. The former requires solution of the dynamical flow equations while the latter requires geometric considerations in addition to a stability analysis. Both provide valuable insight into the variety of fluid interfacial behavior possible over a wide range of α and γ.

3.2.1 DYLCO, Drop Tower, $\gamma \leq \pi/2 - \alpha$; Analysis of Flow.—In low gravity environments the interior corners of partially filled containers can provide a means of dramatic capillary pumping. The flow, bounded by the two walls meeting at the corner and the free surface, is driven by the decrease in radius of curvature along the flow direction. The pressure in the fluid column is less than the ambient by an amount which is inversely proportional to the radius of curvature and so a negative pressure gradient is established. The assumption of slight variation in interfacial curvature in the direction of flow permits an asymptotic analysis of this transient 3-dimensional moving contact line problem.

Provided the condition $\gamma \leq \pi/2 - \alpha$; is satisfied the velocity of liquid motion along a wedge scales as the ratio of the interface tension over the dynamic viscosity, multiplied by a dimensionless geometric factor, which accounts for the dependence of the capillary underpressure on geometry; specifically, on the contact angle γ, the dihedral angle 2α, and the length and characteristic height of the fluid column along the corner. For small contact angles, γ, a high capillary underpressure arises, which results in a fast penetration of the fluid into the wedge, whereas for contact angles close to the limit $\alpha + \gamma \leq \pi/2$ a low capillary underpressure is established which yields slow penetration.

In the following the basic assumption is made that in the planes perpendicular to the wedge the liquid surface is given by a circular section with radius R(z), z being the coordinate in the wedge direction. This principle recently has been successfully applied to the calculation of static liquid surfaces in polyhedral containers [Langbein (1995)]. It has been shown that the liquid surface evolves exponentially from a cylindrical shape along the corner to the spherical shape of the meniscus near the base(s) of the container.

The equation for the simplified flow problem will be developed below. Many details of the complete analysis have been omitted in the interest of brevity and reference should be eventually made to Langbein and Weislogel (1996) for the complete work. The differential equation of liquid penetration into the wedge is obtained by requiring that the change in liquid volume on the side to be filled, that is for $\zeta \geq z$, must equal the flow through the cross-section at z. This volume flow is generally proportional to the squared area of the cross-section times the pressure gradient [Washburn (1921)], yielding

$$\frac{\text{volume}}{\text{time}} = -\frac{c}{\mu}(\text{cross-section})^2 \frac{\partial P}{\partial z} \tag{1}$$

and

$$\frac{\partial}{\partial t}\int_z^\infty d\zeta L_2 R^2 = -\frac{c}{\mu}\left(L_2 R^2\right)^2 \frac{\partial P}{\partial z} \tag{2}$$

L_2R^2 is the area of the local cross-section. The normalized cross-section L_2 equals

$$L_2 = \frac{\cos\gamma}{\sin\alpha}\sin\delta - \delta \quad \text{where} \quad \delta = \frac{\pi}{2} - \alpha - \gamma \tag{3}$$

μ is the dynamic viscosity and c is a friction coefficient, which for the flow in a circular tube, i.e. for the well-known Hagen-Poiseuille flow, equals $1/8\pi$. Differentiation with respect to z on both sides of equation (2) renders

$$\frac{\partial L_2 R^2}{\partial t} = +\frac{c}{\mu}\frac{\partial}{\partial z}\left(L_2 R^2\right)^2 \frac{\partial P}{\partial z} \tag{4}$$

The capillary pressure, under the above assumption of circular cross-sections, is given by

$$P = -\sigma\left(\frac{1}{R} + L_1 \frac{\partial^2 R}{\partial z^2}\left[1 + L_1^2\left(\partial R/\partial z\right)^2\right]^{-3/2}\right) \tag{5}$$

L_1 is the normalized height of the meniscus perpendicular to the wedge axis,

$$L_1 = \frac{\cos\gamma}{\sin\alpha} - 1 \tag{6}$$

Note that $R = h/L_1$, refer to figure 7 for notation. Upon substitution of these quantities into equation (4) we obtain

$$\frac{\partial R^2}{\partial t} = -\frac{c\sigma L_2}{\mu}\frac{\partial}{\partial z}R^4\frac{\partial}{\partial z}\left(\frac{1}{R} + L_1\frac{\partial^2 R}{\partial z^2}\left[1 + L_1^2(\partial R/\partial z)^2\right]^{-3/2}\right) \tag{7}$$

This is a fourth order partial differential equation for R(z,t). equation (7) can also be derived by asymptotic techniques beginning with the Navier-Stokes equations and invoking the lubrication approximation for flow in the positive z-direction. Both developments require low inertia, a slender fluid column and curvature parallel to the z axis much smaller than curvature perpendicular to it. In general, equation (7) has to be solved numerically. On the other hand, it is similar in character to a diffusion equation with the modification of different powers of R(z,t) appearing on its two sides. Equation (7) is an equation in which the effective diffusion coefficient decreases with decreasing cross-section.

Scaling of the time with the velocity σ/μ makes it a length. Scaling of lengths is properly based on the curvature $1/R_{sph}$ in the cylinder ends. It determines the curvature $1/R_{cyl}$ of the cylindrical surfaces in the wedges according to

$$\frac{1}{R_{cyl}} = \frac{2}{R_{sph}} \tag{8}$$

R_{sph} results from the face width L_0 of the prisms used by

$$R_{sph}\cos\gamma = L_0 \quad \cos\alpha\sin\alpha \tag{9}$$

Hence, we scale lengths and time as

$$\tilde{R} = \frac{R}{R_{cyl}} \quad \text{and} \quad 2\tilde{t} = t\frac{c\sigma L_2}{\mu R_{cyl}} \tag{10}$$

This scaling of time is similar to that obtained for the capillary rise in a circular tube. The essential difference is the strong dependence on curvature via the contact angle and the dihedral angle, which enter the normalized cross-section L_2. If the critical wetting condition $\alpha+\gamma = \pi/2$ is approached, L_2 approaches zero proportional to $\delta^2 = (\pi/2 - \alpha - \gamma)^2$. This makes penetration very slow as γ nears $\pi/2 - \alpha$ from below.

Similarity Solutions for Long Times

Let us first assume that the curvature of the meniscus in wedge direction is negligible in comparison to the curvature perpendicular to the wedge direction. This assumption is valid if ample time is allowed for the fluid to extend a sufficient length such that it may be considered a slender column. In that case equation (7) reduces to

$$\frac{3}{2}\frac{\partial R^2}{\partial t} = \frac{\partial^2 R^3}{\partial z^2} \tag{11}$$

where R, t, and z are dimensionless (~'s are dropped for convenience). Equation (11) is equivalent to

$$\frac{\partial R^3}{\partial t} = R\frac{\partial^2 R^3}{\partial z^2}; \quad \frac{\partial R}{\partial t} = 2\left(\frac{\partial R}{\partial z}\right)^2 + R\frac{\partial^2 R}{\partial z^2} \tag{12}$$

Looking for similarity solutions is a most useful concept when trying to solve the diffusion equation. We apply this concept for solving equation (11) which yields similarity under the general substitution

$$R(z,t) = \frac{1}{z^n} f(\eta); \qquad \eta = \frac{z}{(2t)^{1/(n+2)}} \tag{13}$$

Insertion of equation (24) into equation (22) renders

$$\frac{3}{n+2} \frac{1}{\eta^{2n-1}} \frac{df^2}{d\eta} + \frac{df^2}{d\eta^2} \left(\frac{f}{\eta^n} \right)^3 = 0 \tag{14}$$

For arbitrary n, equation (14) has the particular solution

$$f(\eta) = -\frac{1}{5} \eta^{n+2} \tag{15}$$

Exact solutions of equation (25) are obtained for n = 1

$$f(\eta) = -\frac{1}{5} \left(\eta^{4/3} - \eta^3 \right) \tag{16}$$

and for n = –1

$$f(\eta) = \frac{1-\eta}{\eta} = \frac{2t-z}{z} \tag{17}$$

The solution best adapted to the meniscus motion in a wedge however arises for n = 0. Numerical integration of equation (14) for n = 0 shows excellent convergence of $f(\eta)$ for $\eta \rightarrow -\infty$. Using the fact that equation (14) is invariant under the substitution $f \rightarrow f/c^{n+2}$, $\eta \rightarrow \eta/c$, we choose $c = \eta_{tip}$, yielding $\eta_{tip} = 1$, $(df/d\eta)_{tip} = -1/2$ and

$$f(-\infty) = 0.4658\ \ 4677\ \ 4285 \tag{18}$$

$$f(0) = 0.3451\ \ 6330\ \ 0000 \tag{19}$$

With the assumption $d^2f/d\eta^2$, $df/d\eta << f(\eta)$, we obtain from equation (14)

$$\frac{d^2f/d\eta^2}{df/d\eta} + 2\frac{df/d\eta}{f} = -\frac{\eta}{f(-\infty)} \tag{20}$$

Integration over η yields

$$\frac{df}{d\eta} = f_1 \exp\left(-\frac{\eta^2}{2f(-\infty)} \right) \tag{21}$$

$$f(\eta) \approx f(-\infty) + f_1 \int_{-\infty}^{n} d\xi \exp\left(-\frac{\xi^2}{2f(-\infty)} \right) \tag{22}$$

with

$$f_1 = -0.1005\ \ 6331\ \ 0168 \tag{23}$$

This is the expected behavior of a diffusion equation for R^3, in which however the diffusion coefficient decreases with decreasing R. Solutions for n = –1, –0.5, 0, 0.5, and 1 are provided graphically in figure 8. Figure 9 shows the specific case of n = 0.

The solution n = 0 renders a tip motion proportional to $\sqrt{t}$, whereas the solution n = 1 renders a tip motion proportional to t. Computational results for several initial conditions are shown in figure 10. In all physically relevant cases, the solution n = 0 eventually dominates the solution as is demonstrated in figure 11 for the linear and parabolic initial surface profiles, respectively. [Note: If instead of putting $\eta_{tip} = 1$, we scale $f(-\infty) = 1$, we obtain $f(0) = 0.740937$ and $\eta_{tip} = 1.465138$.]

Noting that η_{tip} = const., the tip location may be expressed in closed form as

$$z_{tip} = \left[C(t + t_o)\right]^{1/2} - z_o \tag{24}$$

the general form of which was successful in correlating the drop tower data of figure 6. It can be shown [Langbein and Weislogel (1996)] the above may be redimensionalized producing

$$z_{tip} = \sqrt{3\frac{c\sigma L_2 R_{cyl}}{\mu}(t + t_o)} - z_o \tag{25}$$

from which the tip velocity may determined to be

$$z_{tip} = \sqrt{\frac{3c\sigma L_2 R_{cyl}}{4\mu(t + t_o)}} \tag{26}$$

where c is a constant which can be computed numerically or measured experimentally. For fixed σ, μ, and c, from equation (26) it can be shown that the penetration rate of the fluid into the corner follows a relationship much like

$$V_{tip} \sim \sqrt{L_2 R_{cyl}} \sim \sqrt{\sin\delta\cos\alpha - \frac{\delta\sin\alpha\cos\alpha}{\sin(\alpha + \delta)}} \tag{27}$$

Clearly, $V_{tip} \to 0$ as $\gamma \to \pi/2 - \alpha$ as $V_{tip} \sim \delta \cos\alpha / \sqrt{\sin\alpha}$ as well as with increasing time. The fact that $V_{tip} \sim \sqrt{\sigma / \mu}$ from equation (26) explains the drop tower findings of the tip velocity increasing with increasing temperature. Since the decrease in surface tension (the driving force for the flow) with temperature is less than the decrease in viscosity (retarding force) with temperature (refer to table I) this aspect of the flow comes as no surprise .

3.2.2 DYLCO, BDPU IML-2; $\pi/2 - \alpha < \gamma < \pi/2 + \alpha$. Stability Analysis

For the limit of zero gravity, the theory to predict the interface shapes generated during the IML-2 mission is well established and incorporates the use of the Young-Laplace equation with constant volume and contact angle boundary conditions. These surfaces are (or should be) surfaces of constant mean curvature which, in Case II, are portions of spherical surfaces. However, for the case of finite gravity ('gravity' being synonymous with 'acceleration level') such surfaces are subject to marginal stability limits determined by the Bond number ($Bo = \rho g L^2/\sigma$, where gravity is taken in the direction of the negative density gradient along the vessel principal axis), which serves as the relative measure of gravitational forces to those of surface tension. For Bo values above a certain critical value, Bo_{cr}, the surface will become unstable leading to break up and flow to another region of the container.

A critical Bond number stability analysis was performed in collaboration with K.C. Hsieh at NASA Lewis Research Center. This analysis required the numerical solution of the Young Laplace equation for the surface elevation S with the constant volume and contact angle constraints for a rhombic vessel with $\alpha = \pi/4$, namely

$$\nabla \cdot \frac{\nabla S}{\sqrt{1+|\nabla S|^2}} = \mathrm{BoS} + \mathrm{const.}$$

subject to the contact angle condition at the contact line

$$\frac{\nabla S}{\sqrt{1+|\nabla S|^2}} \cdot \mathbf{k} = \cos\gamma$$

where Bo is based on length scale L, the half width of the smallest side of the container, the constant arises form the particular selection of fluid volume, and **k** is the unit inward normal of the container wall. All lengths have been nondimensionalized by L. The numerical solution technique employed a second order accurate finite difference formulation on a nonuniform grid. It was found that a large concentration of nodes was necessary to accurately capture the correct curvature of the interface in the corner as the contact angle approached the critical value of $\pi/2 - \alpha$. At this point the fluid interface becomes increasingly vertical making numerical resolution difficult. An 80×80 grid was used for the majority of the calculations with 100×100 providing minimal improvement.

The marginal stability curve for the case of $\alpha = \pi/4$ is presented in the figure below for Bo_{cr} as a function of contact angle.

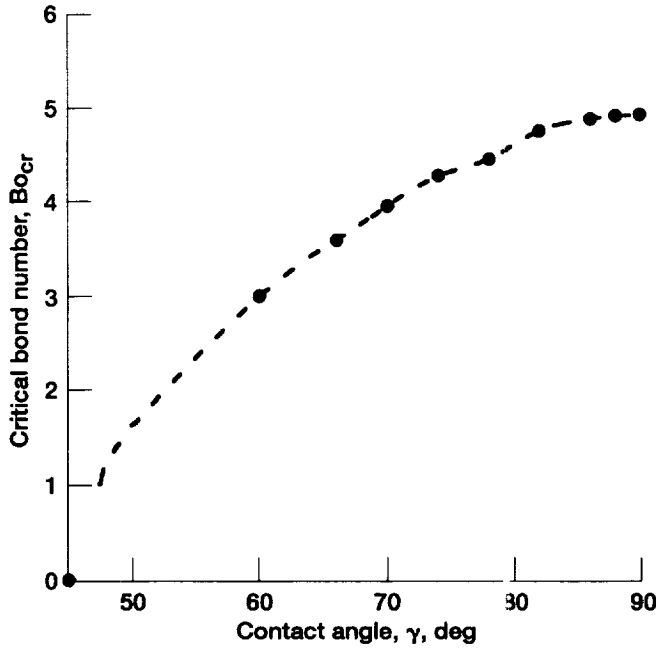

Inspection of the above shows increased stability for increasing contact angles up to $\gamma = 90°$. An analytical result was possible for Bo_{cr} at $\lambda = 90°$ following the derivation of Maxwell (1890) only employing the complete slip model at the contact line.

It is interesting to note that not only does the stability decrease an order of magnitude between $\gamma = 90°$ and $\gamma = 46°$, but that Bo_{cr} drops abruptly to 0 as γ approaches $\pi/2 - \alpha$. The singular point of $\gamma = \pi/2 - \alpha$ is the critical juncture between Cases I and II outlined above and is the critical angle identified by Concus and Finn (1974) at which stable solutions cannot exist which cover the base of a container of semi infinite extent. In other words, the liquid volume covers the base while the liquid surface does not. From a theoretical perspective, an infinitesimal but steady disturbance to the cell would disrupt any fluid interface where γ is slightly greater than the critical value of $\pi/2 - \alpha$.

4. RESULTS AND COMPARISONS

As was previously stated, for the case of $\pi/2 - \alpha < \gamma < \pi/2 + \alpha$, the resulting surfaces are portions of spherical surfaces. It is this feature of the surfaces achieved on orbit which allowed for their easy characterization since by knowing the radius of curvature of the surfaces from the film records, the angle of intersection of the surface and the wall in the plane of the photographs could be transformed simply to give the contact angle for the particular cell at temperature. This was accomplished via the geometric relationships

$$\cos\phi = W / R \quad \text{and} \quad \cos\gamma = \cos\phi\cos\alpha \tag{28}$$

where W is the half width of the cell from the perspective of the camera and R is the radius of curvature, assumed constant, of the interface in question. Refer to the figure below for notation.

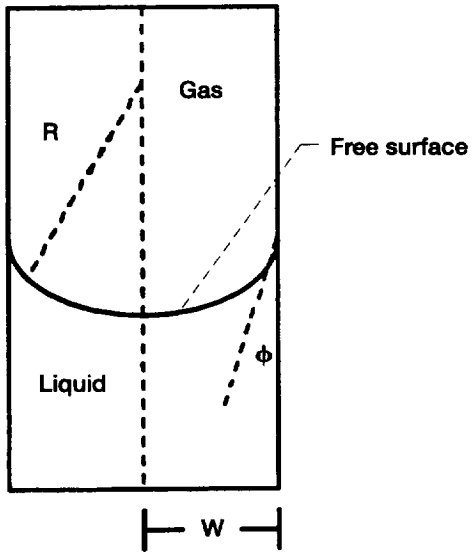

R was determined by curve fitting the digitized surface to the following form

$$(x-a)^2 + (y-b)^2 = R^2 \tag{29}$$

which is the equation of a circle centered at x = a, y = b. a, b and R could be determined from the fit and the degree of precision was a direct indication of the degree of sphericity of the interface. The constant a could also be input since it was known experimentally, but doing so produced little effect to the fit results for R. A sample of values for γ determined in this way is provided in table II for surfaces digitized at four select time increments: (1) after fill and prior to heating, (2) an arbitrary point during the heating steps, (3) at the peak temperature, and (4) at the termination of the experiment after cooling.

In all but case (4) it is possible to fit the curves with a portion of a circle and to determine the contact angle. The data selected above for cells 3 and 4 appear to exhibit somewhat anomalous behavior as compared to cells 1 and 2, a contributor to which could be the familiar sporadic 'stick-slip' nature of fluid motion at the contact line.

The changes in interface shape between one heating step and another was ruled by the fact that the fluid expanded (contracted) with increase (decrease) in temperature. Due to the contact angle hysteresis present, relatively minor motion of the contact line was detected during a temperature step with the change in fluid volume being accommodated primarily by the change in interface curvature alone. Surprisingly, the hysteretic angles remained constant around the contact line for the majority of the tests. This allowed the measurements of the effective contact angles in these instances, increments 1, 2, and 3 of table 2. As pointed out, however, for increment 4 shown in table 2, a non-uniform contact angle distribution about the contact line was observed yielding a more parabolic interface as opposed to a spherical shape. This is similar to the hysteresis effects of a drop of water on a tilted plate, albeit on a larger length scale. No theory developed to date is known to predict such surfaces, let alone their stability, as information as to the history of the fluid is neces-

sary in addition to quasi-equilibrium constitutive data on the hysteretic behavior of the fluid-solid pair. Models incorporating variable contact angle distributions at the contact line may serve well in this regard. Local contact angle measurements in the vertices of the cells at increment 4 show that the receding limit is reached in the corner since γ_{rec} is approximately 40° at room temperature. This point is very intriguing and will be discussed further.

It is important to note that surfaces as in increment 4 do not arise commonly in simple rotationally symmetric containers such as the right circular cylinder, annulus, and sphere. Hysteretic values of the contact angle for vessels of these geometries are predominantly uniform about the contact line since the bulk fluid motion is, in general, perpendicular to the contact along its entirety. This is not the case for the rhombic sections studied here where fluid motion is only perpendicular to the contact line at several singular points (at each vertex and at one location on each vertical face).

The effect of hysteresis on the fluid behavior due to thermal expansion was anticipated. A freshly coated surface produces little hysteresis (at times less than approximately ±2°), but aging of the surface and exposure to a normal laboratory environment act gradually to produce a much larger, though repeatably measurable, range of values. Higher cleanliness requirements can reduce the hysteresis limits of the advancing and receding contact angle limits. Unfortunately, the techniques necessary (i.e. on board coating, UHV chamber, on board cleaning with solvents, etc.) required prohibitive measures with regard to safety as well as expense. The test cells of DYLCO were coated and stored in the sealed test containers under ambient conditions for 3 (?) months prior to launch. Agreement of the receding contact angles measured from the flight tests with the ground based lab measurements indicates that no further contamination, beyond that which can be easily reproduced in the laboratory with routine precautions, of the containers or fluid took place.

Regardless of the presence of hysteresis, however, for measurements on the ground, spurious and/or intentional disturbances in addition to ample time, act to relieve the stresses at the contact line and allow the establishment of a more equilibrium value of the contact angle. Disturbances and/or time of sufficient magnitude was not present during the IML-2 mission for such relaxation at the contact line to occur and a general increase, rather than decrease, of the contact angle, counter to intuition, was measured with increasing temperature.

What is perhaps most interesting about the results in table II, cells 1 and 2 in particular, is that the critical wetting condition was exceeded by a hysteretic surface curvature. What resulted were stable interfaces of the type outlined as Case II. The figure below displays the digitized profile of the interface in cell 1 at time increments 1 to 4.

Traces of interface curvature for Cell 1 at select time increments. Symbols are data, lines are circular fits. x and y are in mm and W for this cell is 5.09 ± 0.15 mm. Shifts left to right are an artifact of the data collection procedure, and ϕ is shown graphically as used for the local determination of γ for the nonspherical surfaces observed at time increment 4.

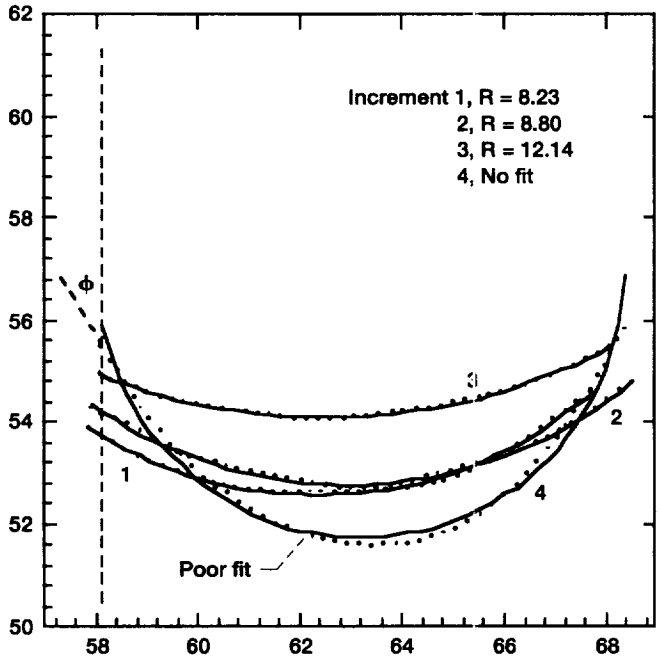

One can see from this figure the degree of fit according to equation (29). Since the surface is not spherical at increment 4 the local slope of the interface at the wall could be measured (see figure) and the local contact angle could be approximated by the transformation of equation (28). These are the contact angle values in table II for increment 4. The results agree closely with the measured value for the receding contact angle given in table I. These contact angle values are well below the critical angle yet no flow, even local, was observed!

The analytic solutions given in Section 3 show conclusively that not only is complete instability reached as the contact angle decreases to the critical condition $\gamma = \pi/2 - \alpha$, but that an infinite amount of time is necessary for the flow to be established once γ first becomes less than $\pi/2 - \alpha$. This is because the driving force for the transition at the transition point is also approaching or equal to zero. It is not surprising that such forces may not manifest themselves in the presence of finite hysteresis which acts to resist interface motion until a threshold capillary pressure is exceeded.

When γ is appreciably less than $\pi/2 - \alpha$ application of the results of Section 3.2.1 are appropriate which show that velocities decrease to zero at a significant rate within 2° of the critical value. One might conclude that hysteresis of this order or greater may swamp such a sensitive critical corner wetting phenomena. Since large hysteresis occurs often in real systems where large contact angles are present one should be particularly aware of the variety of behaviors one might expect.

The fact that no flow occurred during the flight tests for surfaces exceeding the critical curvature for critical wetting may possibly be explained by the fact that the equilibrium value of the contact angle had still not exceeded the critical limit for the particular cell (refer to tables 1 and 2). This conclusion gives no explanation how such surfaces could be stable, but it does allow for critical wetting, in accord with the theory, if the temperature were higher (lower γ) or the wedge dihedral angles were smaller (lower α).

5. CONCLUSIONS, SIGNIFICANCE, AND FUTURE PLANS

Analyses predicting both the flow properties for surfaces satisfying $\gamma \leq \pi/2 - \alpha$ and the stability limits for a selected case of $\pi/2 - \alpha < \gamma < \pi/2 + \alpha$ are presented which illuminate the sensitive nature of flows/surfaces near the critical wetting transition $\gamma \leq \pi/2 - \alpha$. The DYLCO experiment performed on IML-2 investigated the impact on changing contact angle for the case $\pi/2 - \alpha < \gamma < \pi/2 + \alpha$. Data were recorded which revealed the effects of contact angle. The results of the analysis and flight experiment data reveal the potentially significant role of contact angle hysteresis in swamping out capillary effects such as the critical corner wetting phenomena occurring when $\gamma = \pi/2 - \alpha$.

Most astonishing about the experimental results was that in every cell tested the critical wetting condition was exceeded by a hysteretic surface curvature (Case I surfaces). Rather than fluid reorientation at this point, what resulted were stable interfaces of the type outlined as Case II. These results can simply not be addressed by present theory which can find no solution for such a condition.

For the case of flow the result of the similarity analysis yields solutions which are of particular interest. For instance, the moving contact line condition is accounted for naturally through a geometric drag coefficient c, though the velocity at the tip is zero it nevertheless moves, and the slope of the interface has a nonzero value at the tip irrespective of the value of the contact angle. These characteristics of the flow are often artificially required in other models, but they arise naturally from equation (7). The reason is the higher power of R on the left-hand side of equation (7) than on the right-hand side. We have

$$R\frac{\partial R}{\partial t} = R\left[2\left(\frac{\partial R}{\partial z}\right)^2 + R\frac{\partial^2 R}{\partial z^2}\right] \tag{30}$$

and divide by R = 0, yielding

$$\frac{\partial R}{\partial t} = 2\left(\frac{\partial R}{\partial z}\right)^2 + R\frac{\partial^2 R}{\partial z^2} = 2\left(\frac{\partial R}{\partial z}\right)^2 \tag{31}$$

Decreasing diffusion with decreasing meniscus accounts for the unique characteristics of the flow at the tip. equation (7) belongs to the class of porous media equations [Friedman (1982)].

The numerical solution confirms a similarity solution at long times t and renders the inherent constants. The general relation for the tip position, experimentally and theoretically, is

$$z_{tip} + z_o = \sqrt{C(t + t_o)} \tag{32}$$

It is also worthy of mention that the driving force for flow is $O(R^{-1})$ while the viscous resistance to the flow is $O(R^{-2})$. Thus, as $R \rightarrow 0$ at the tip an infinite force is available to alleviate the mathematical difficulties of the no slip condition (infinite resistance) applied there.

Solutions provided in Section 3 show that key features of the flow can be determined in closed form. These include the tip location and velocity, the slope of the interface at the tip, the flow rate of fluid along the corner, and the surface shape, all in terms of the fluid viscosity, surface tension, contact angle, corner angle and vessel size. These results are immediately useful in the prediction of related flows.

Because of its relevance to applications and interest to scientists, research will continue on related topics concerning the behavior of fluid interfaces in containers of irregular geometries. In the past such studies have included numerous ground tests and parabolic flights [Langbein (1990)]. DYLCO was the first flight experiment devoted specifically to this topic and two others are soon to follow: A study similar in approach to DYLCO is planned for Flight aboard the shuttle during the USML-2 mission which maintains constant contact angle while varying the corner half angle, α. The experiment is called the Interface Configuration Experiment-Wedge vessel [Concus et al. (1995)] and is slated to fly in October, 1995. Another related study of the effect of rotation on the behavior of fluid interfaces in irregular vessels is planned for the MAXUS sounding rocket in November, 1995. Other relevant studies investigate the effects of heat transfer and intermolecular surface forces [Chan (1994), DasGupta et al. (1994)]. With results of DYLCO and the experiments named above, a great deal has been and will be learned about the nature of fluids in partially fluid filled containers possessing interior corners. Since such surfaces arise in many contexts, particularly regarding in-space fluids systems, much predictive capability has been added to our fundamental understanding of capillary surfaces and flows.

REFERENCES

Cahn, J.W.: J. Chemical Physics, 1977, vol. 66(8), p. 3667.

Chan, S.H.: Experimental and Theoretical Studies of Rewetting of Unheated/Heated Grooved Plates, Second Microgravity Fluid Physics Conference, Cleveland, OH, June, 1994. NASA CP–3276, p. 241.

Concus, P., Finn, R., Weislogel, M.: Interface Configuration Experiment, A Glovebox experiment for USML-2, Brochure, B-0809, Aug. 1995.

Concus, P., Finn, R.: Capillary Surface in Microgravity, in Low-Gravity Fluid Dynamics and Transport Phenomena, Vol. 130, Progress in Astronautics and Aeronautics, AIAA, 1990, pp. 183–204

Concus, P., Finn, R.: On Capillary free surfaces in the absence of gravity, Acta Math., Vol. 132, 1974, pp. 177–198.

DasGupta, S., Plawsky, J.L., Wayner, P.C., Jr.: Interfacial Force Field Characterization of a Constrained Vapor Bubble Thermosyphon Using IAI, Second Microgravity Fluid Physics Conference, Cleveland, OH, June, 1994. NASA CP–3276, p. 253.

Friedman, A.: Variational Principles and Free Boundary Problems. Wiley, New York (1982). Porous Media Equation: Eine Zusammenfassung wichtiger Resultate ist zu finden in.

Langbein, D., Weislogel, M.M.: Capillary Driven Flows in Corners, 1996 (in preparation).

Langbein, D., Groβbach R, Heide W: Parabolic Flight Experiments on Fluid Surfaces and Wetting. Appl. Microgravity Techn. II (1990) 198–211.

Langbein, D.: The shape and stability of liquid menisci at solid edges. J. Fluid Mech. 213 (1990) 251–265.

Langbein, D.: Liquid surfaces in polyhedral containers. Robert Finn Conference Proceedings. P. Concus, K. Lancaster (eds.) International Press, Cambridge (1994) pp. 168–173.

Maxwell, J.C.: Scientific Papers of James Clerk Maxwell, Chpt. LXXXIII. Capillary Action, Cambridge University Press, London, 1890.

Rollins, J.R., Grove, R.K., Jaekle, D.E., Jr.: Surface Tension Propellant Management Systems for Aerospace Vehicles, International Symposium on Space Technology and Science, 15th, Tokyo, Japan, May 19-23, 1986, Proceedings, Vol. 1, pp. 177–188.

Washburn, E.W.: The Dynamics of Capillary Flow. Phys. Rev. 2nd Series XVII 3 (1921) pp. 273–283.

Weislogel, M.M., Lichter, S.: Capillary Driven Flow in Containers with Interior Corners in Low Gravity (Preprint).

Specific Publications/Presentations Concerning DYLCO

Publications:

Langbein, D.: Liquid surfaces in polyhedral containers. Robert Finn Conference Proceedings. P. Concus, K. Lancaster (eds.) International Press, Cambridge (1994) pp. 168–173.
Langbein, D.: Liquid surfaces in polyhedral containers. Microgravity sci. technology (to appear).
Langbein, D., Weislogel, M.M.: Capillary Driven Flows in Corners, 1996 (in preparation).
Weislogel, M.M., Lichter, S.: Capillary Driven Flow in Containers with Interior Corners in Low Gravity (in preparation).
Weislogel, M.M., Hsieh, K.C.: Stability of Capillary Surfaces in Irregular Containers (in preparation).

Presentations:

Langbein, D.: Preliminary Report of July, 1994, on the performance of the IML-2 Experiment DYLCO.
Weislogel, M., Lichter, S.: Capillary Driven Flow in a Wedge in Low Gravity, American Physical Society Meeting of the Division of Fluid Dynamics, BA3, Abluquerque, NM, November, 1993.
Weislogel, M.M., Lichter, S.: Low Gravity Capillary Flow in a Corner, American Physical Society Meeting of the Division of Fluid Dynamics, CA1, Atlanta, GA, November, 1994.

TABLE 1.—RELEVANT THERMOPHYSICAL PROPERTIES FOR CARGILLE FLUID 30350, FUSED SILICA INDEX OF REFRACTION MATCHED N = 1.4587 AT 25 °C (@5893ANGST.).ALL CONTACT ANGLE MEASUREMENTS ARE ACCURATE TO ±2° WITH REPEATABILITY GIVING UNCERTAINTIES OF ±3°. EQUILIBRIUM CONTACT ANGLES ARE 70° AT 20 °C AND 65° AT 100 °C

Temperature, °C	ρ, kg/m^3	Temperature, °C	μ, $\times 10^{-3}$ kg/ms
23.2	835	19.9	16.43
43.6	816	40.0	8.41
60.9	799	60.0	5.03
78.2	781	80.0	3.36
		100.0	2.42

Temperature, °C	σ, N/m	Temperature, °C	γ_{adv}, deg	Temperature, °C	γ_{rec}, deg
19.7	0.0297	21.0	82.1	20.7	40.0
39.6	.0287	40.0	80.6	40.1	37.5
59.3	.0277	60.1	80.6	60.1	37.5
77.9	.0262	100.0	77.5	80.1	40.5
96.4	.0252	119.6	74.4	100.2	45.3
		139.8	71.3	120.3	45.3
		166.6	68.3	139.9	48.0
		179.7	68.3	160.1	50.8
		199.5	65.3	200.1	48.0

TABLE II.— CONTACT ANGLES AS OBTAINED BY INTERFACE DIGITIZATION IN THE PLANE PERPENDICULAR TO THE LINE OF SIGHT AND CONTAINING THE VERTICES OF THE CORNERS WITH THE LARGER HALF ANGLE. FOR INCREMENT 4 LOCAL CONTACT ANGLES MEASURED IN THE NEAR VICINITY OF THE VERTICES OF THE VESSELS ARE TABULATED.

	γ at increment # (±2 deg.).				
	1	2	3	4 ($R \neq$ const.)	γ_{cr} for cell
Cell 1	51.7	54.6	65.2	42.7	60.0
Cell 2	50.3	52.3	64.8	42.5	57.5
Cell 3	70.0	44.9	80.8	41.1	55.0
Cell 4	60.7	65.7	72.8	50.7	52.5

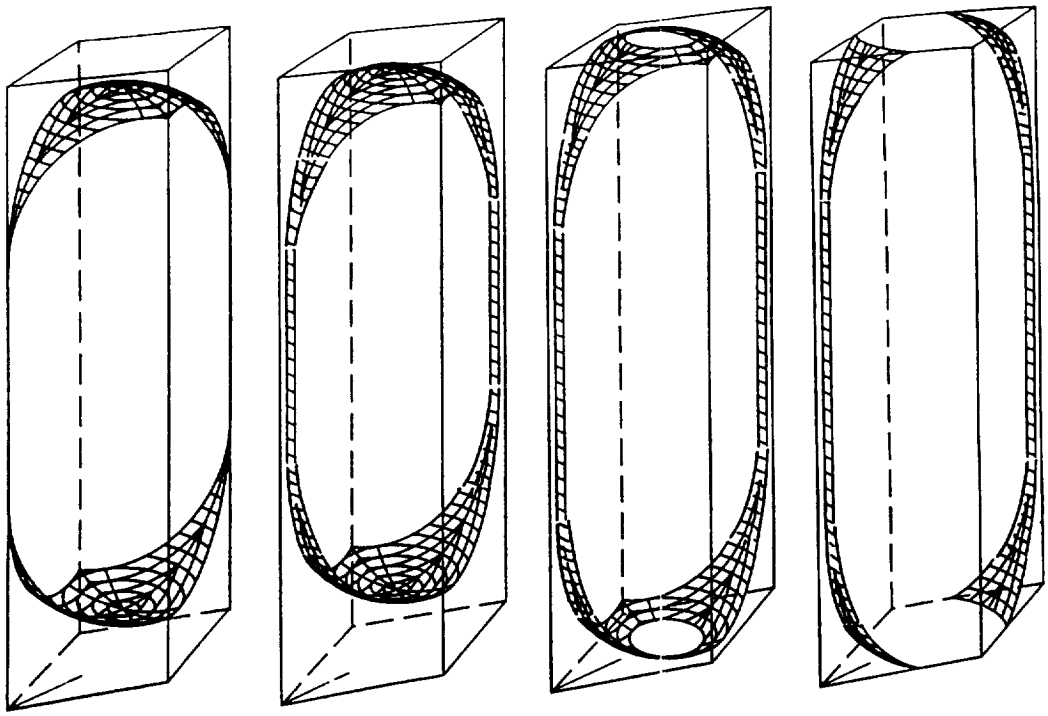

Figure 1.—Liquid surfaces in rhombic prisms for various contact angles γ dihedral angles 2α.

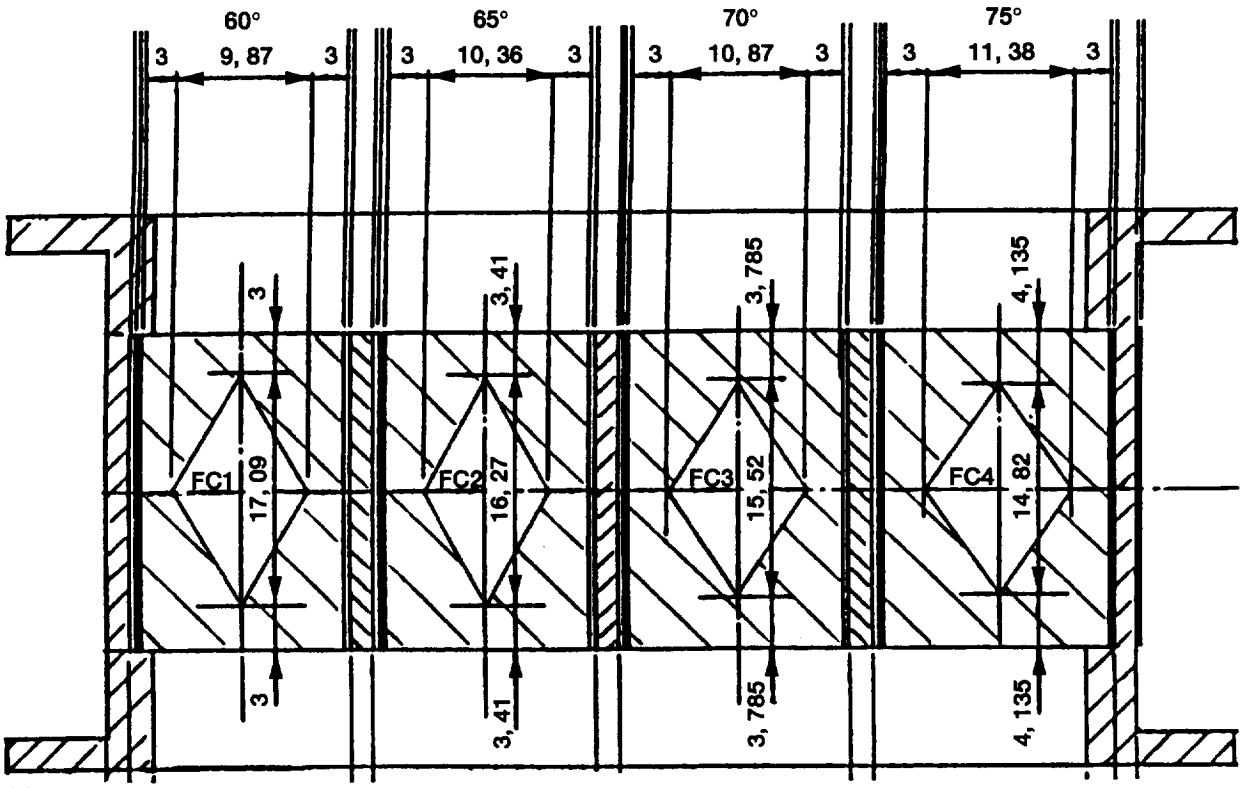

(a)

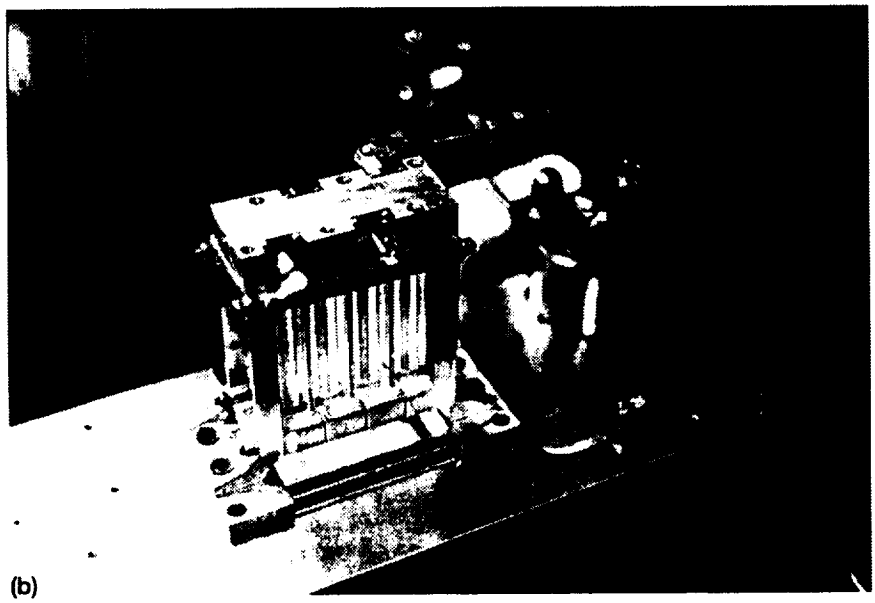

(b)

Figure 2.—(a) Schematic of the test cell cross sections for DYLCO. (b) Photograph of DYLCO flight hardware.

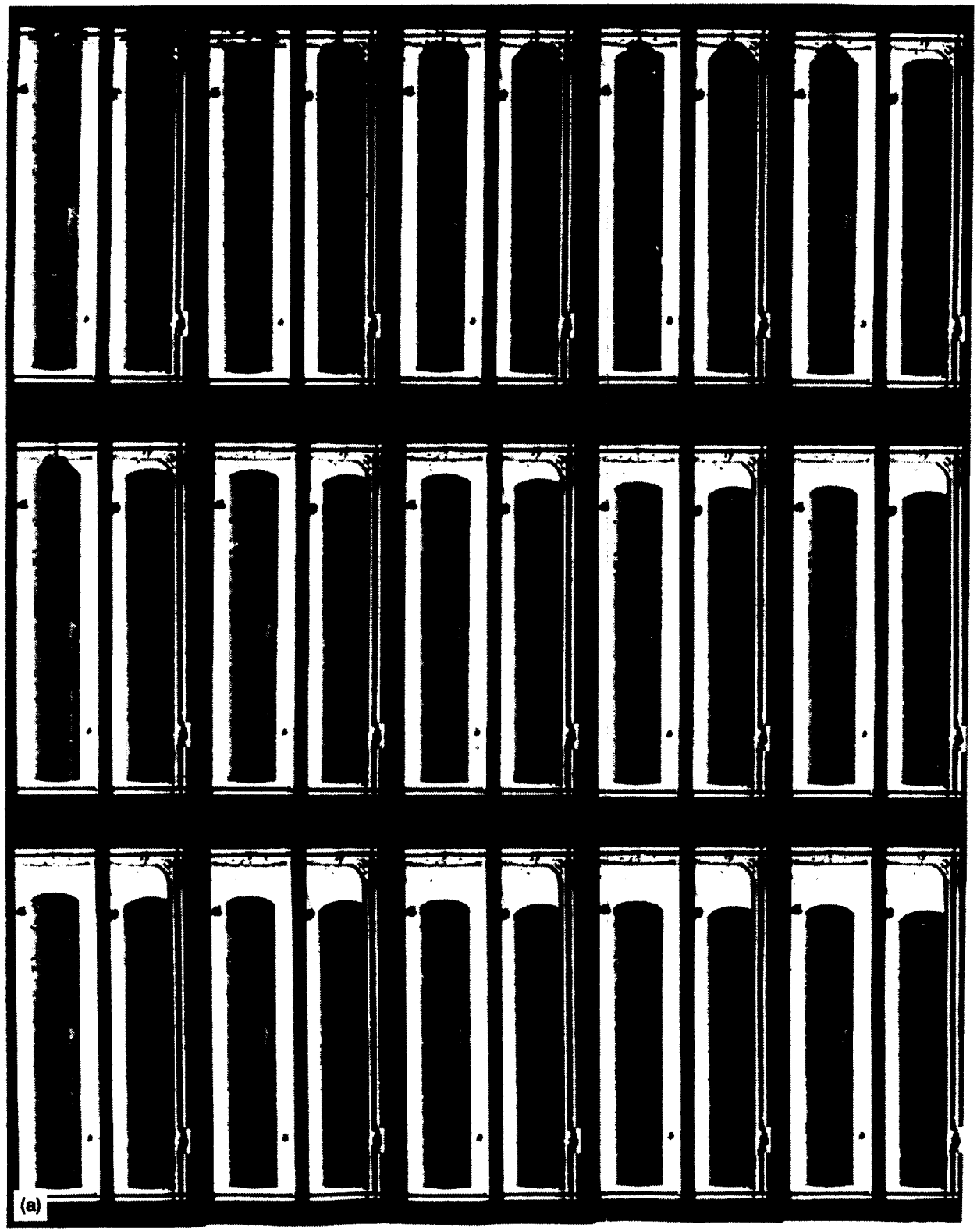

Figure 3.—IML-2 experiment data. (a) Filling of the right-hand cells with dihedral angles $2\alpha = 65°$ (left) and $2\alpha = 60°$ (right). The time interval between subsequent picture is 4s. (b) During heating up to 40, 60, 80, 90 and even 95 °C. (c) During cooling down to 90, 80, 60, 40 °C and ambient temperature.

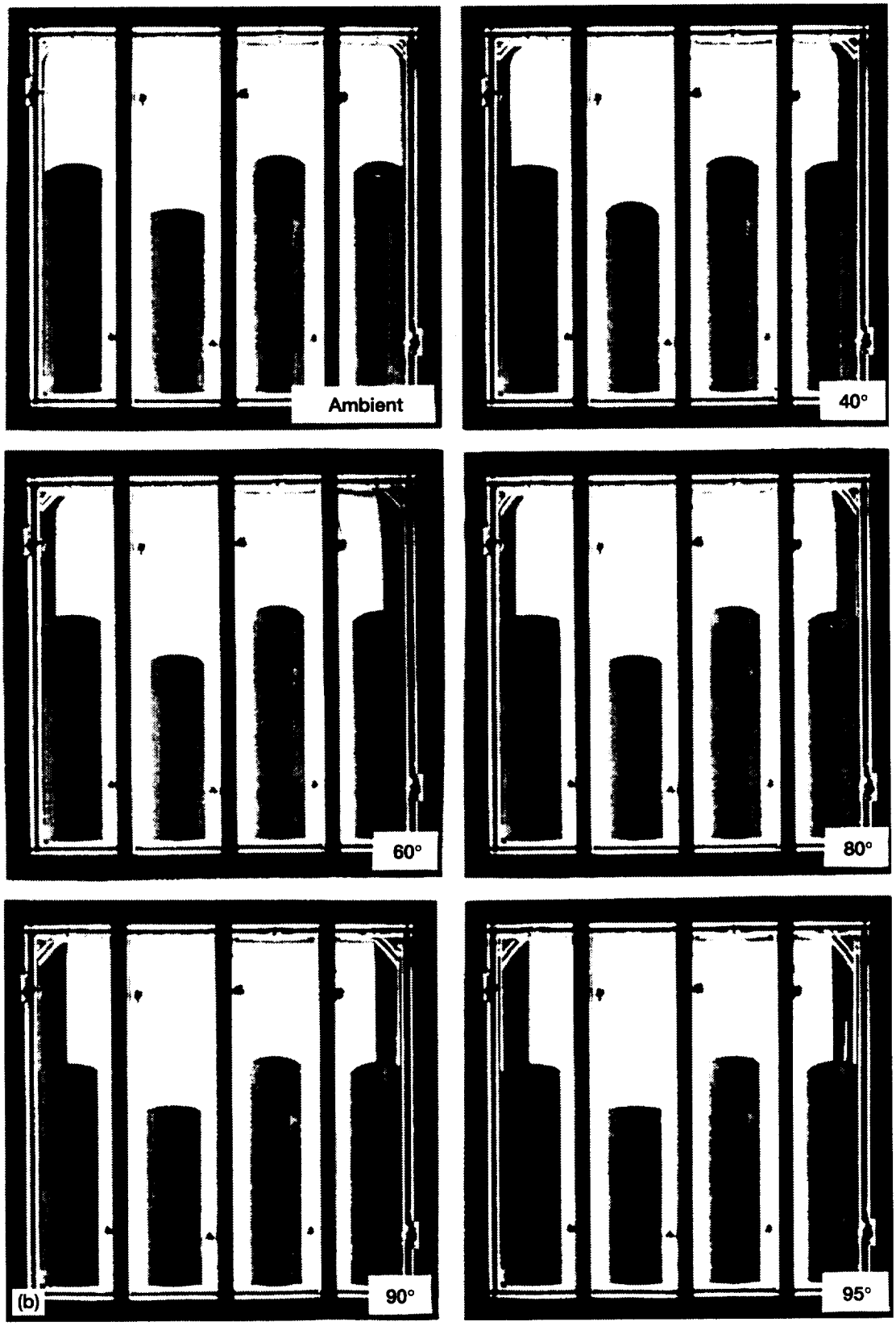

Figure 3.—Continued. (b) During heating up to 40, 60, 80, 90 and even 95 °C.

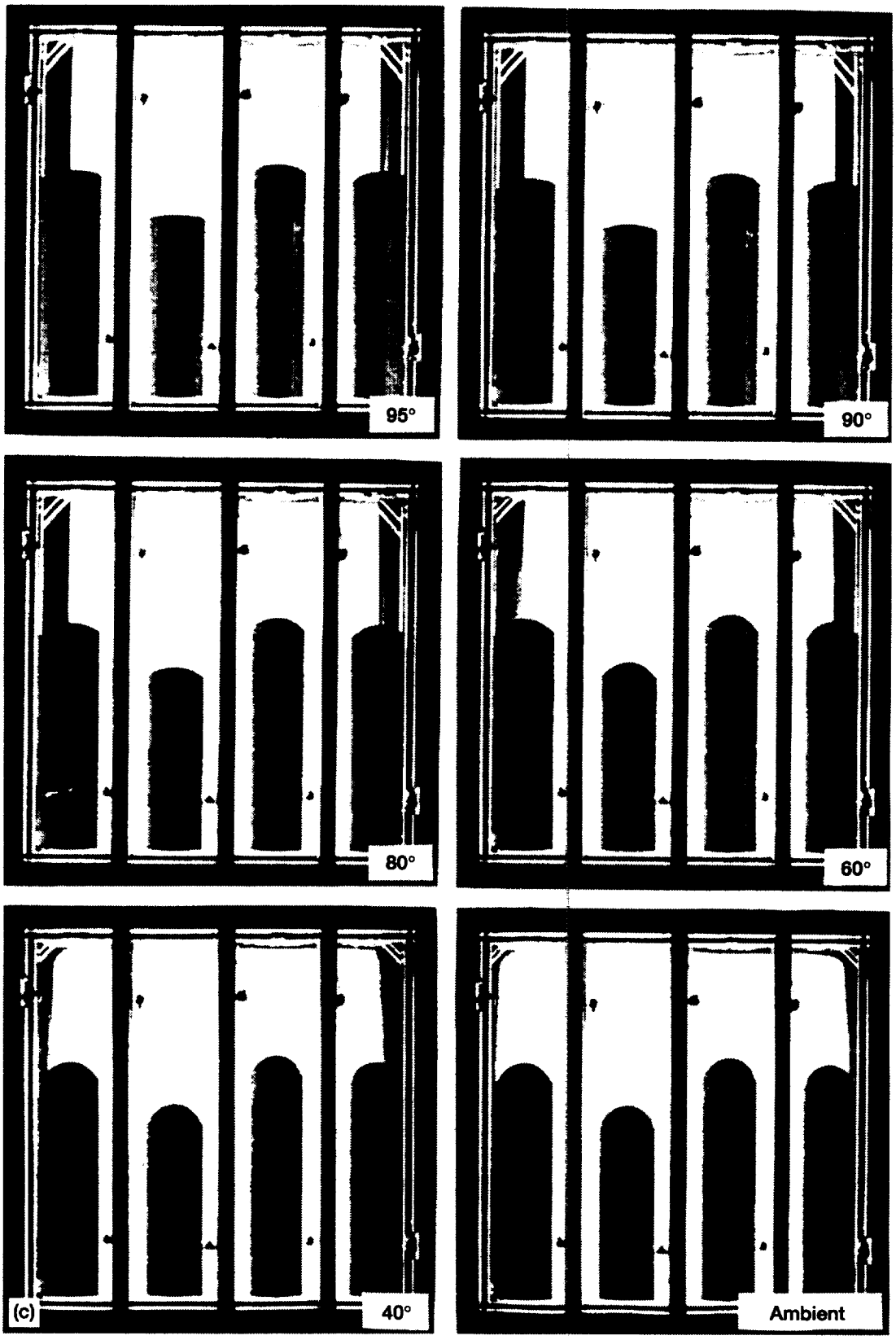

Figure 3.—Concluded. (c) During cooling down to 90, 80, 60, 40 °C and ambient temperature.

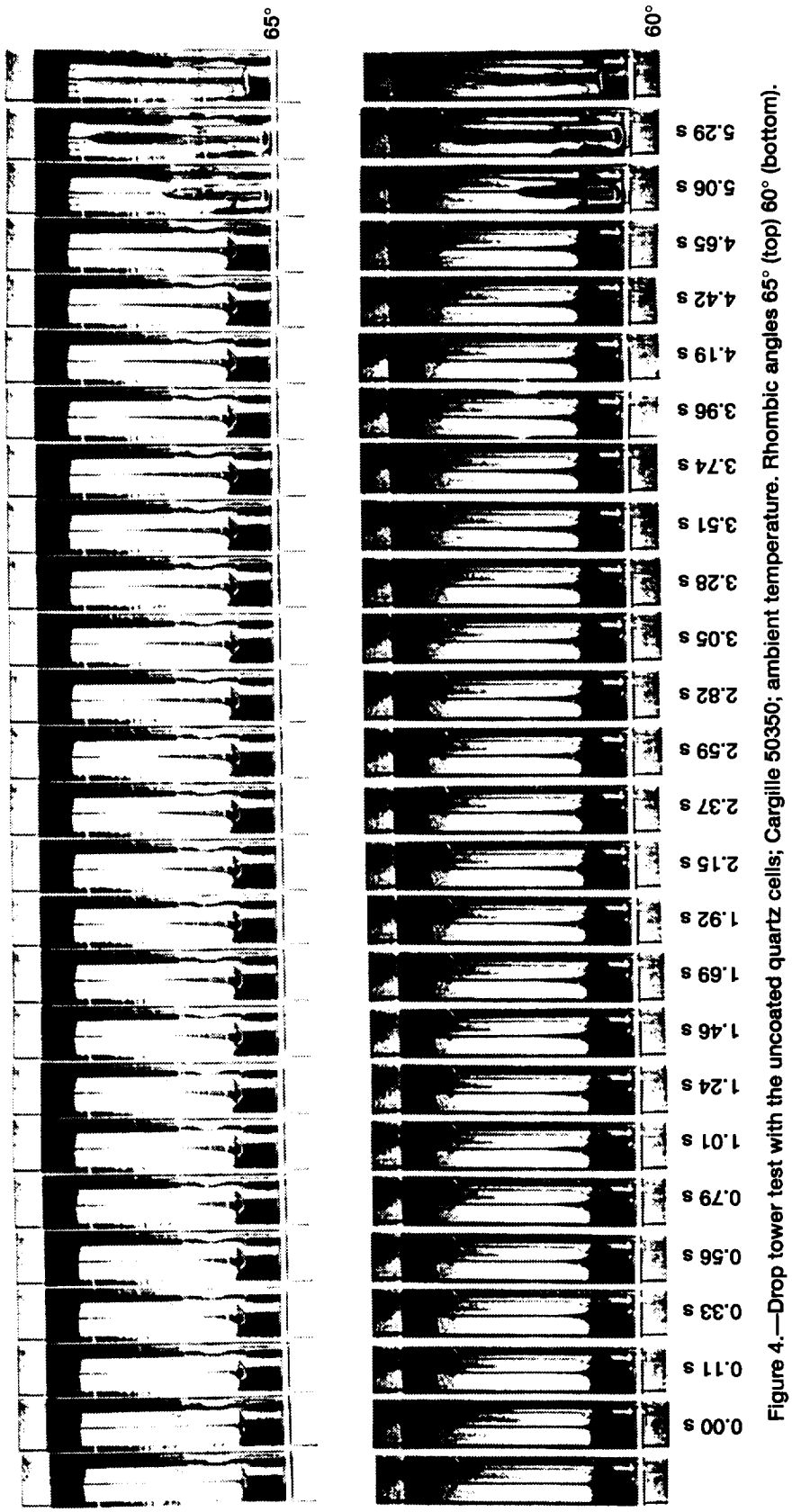

Figure 4.—Drop tower test with the uncoated quartz cells; Cargille 50350; ambient temperature. Rhombic angles 65° (top) 60° (bottom).

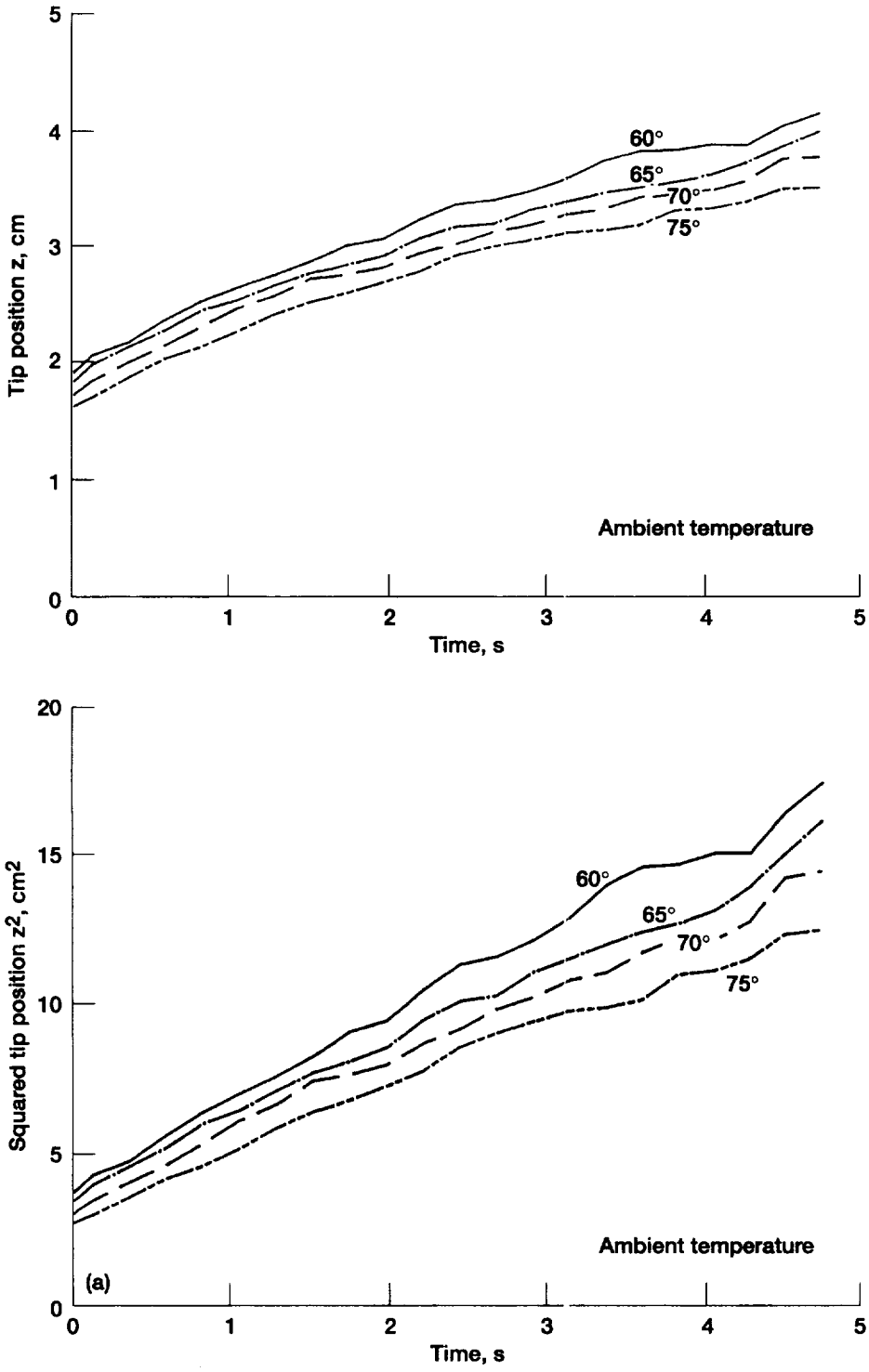

Figure 5.—Tip position z versus time t in the drop tower tests. The squared tip position rises approximately linear in all cases. Due to the decrease in viscosity the spreading velocity clearly increases temperature. (a) Ambient temperature. (b) T = 40 °C. (c) T = 60 °C.

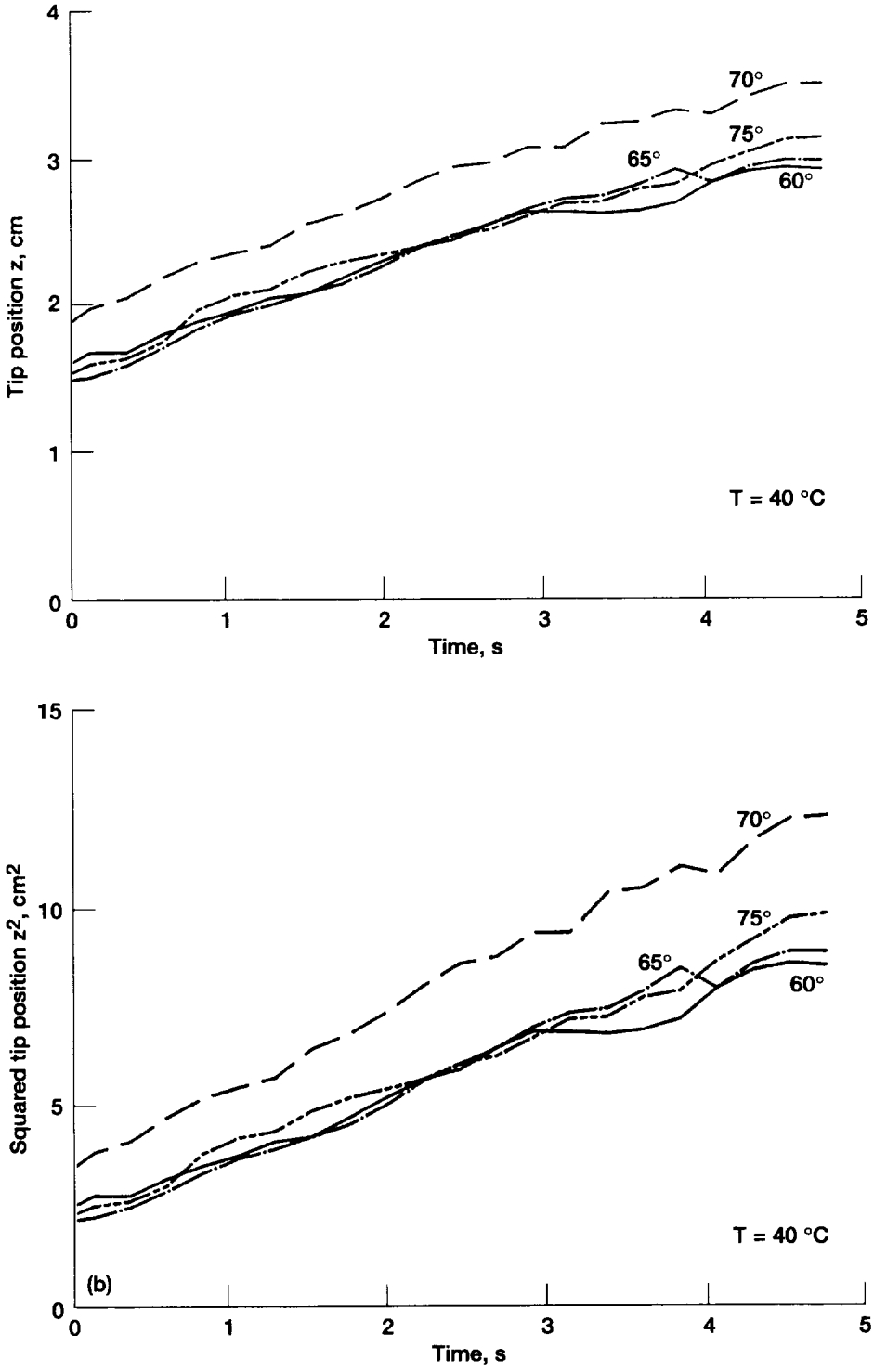

Figure 5.—Continued. (b) T = 40 °C.

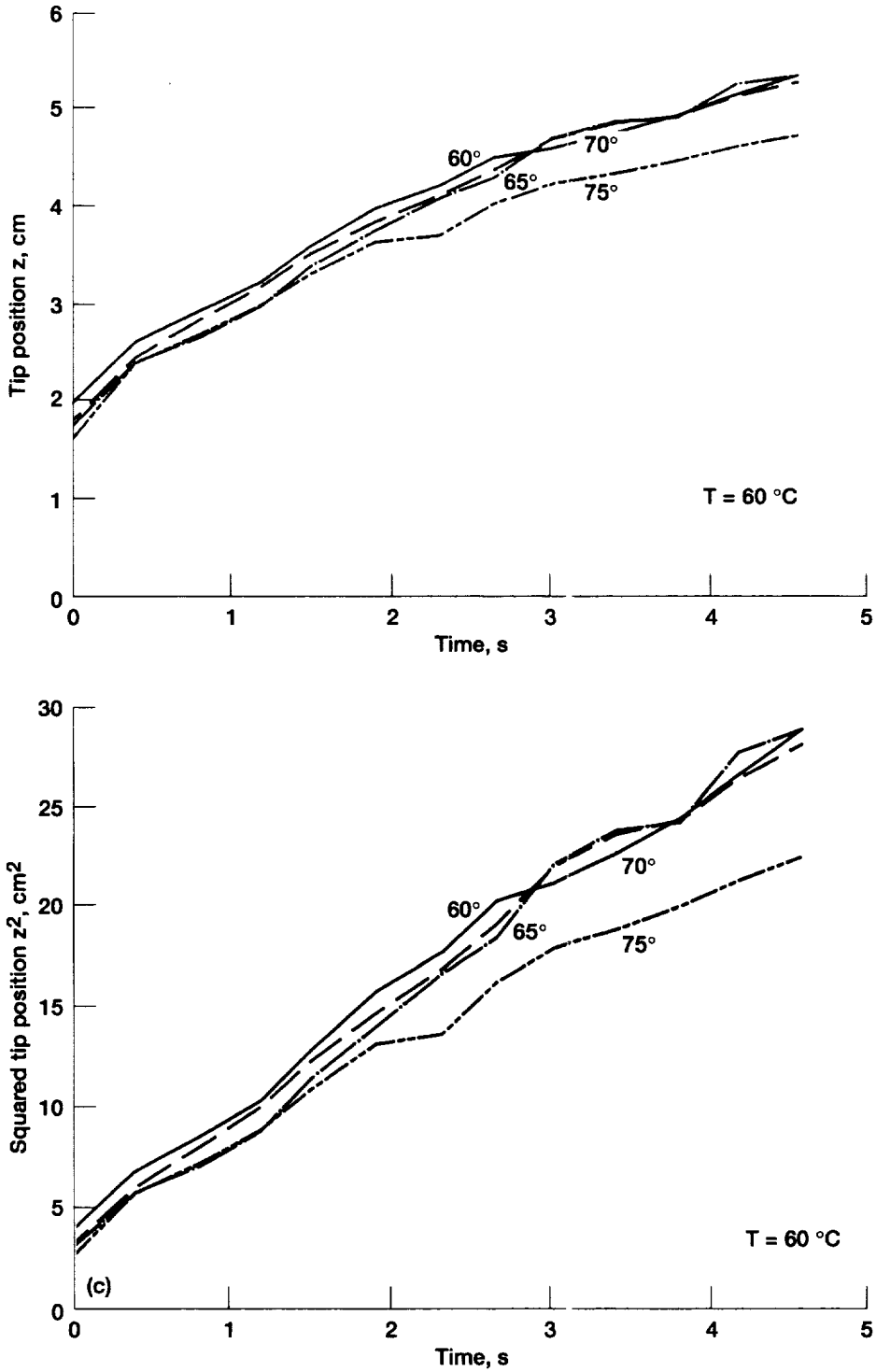

Figure 5.—Concluded. (c) T = 60 °C.

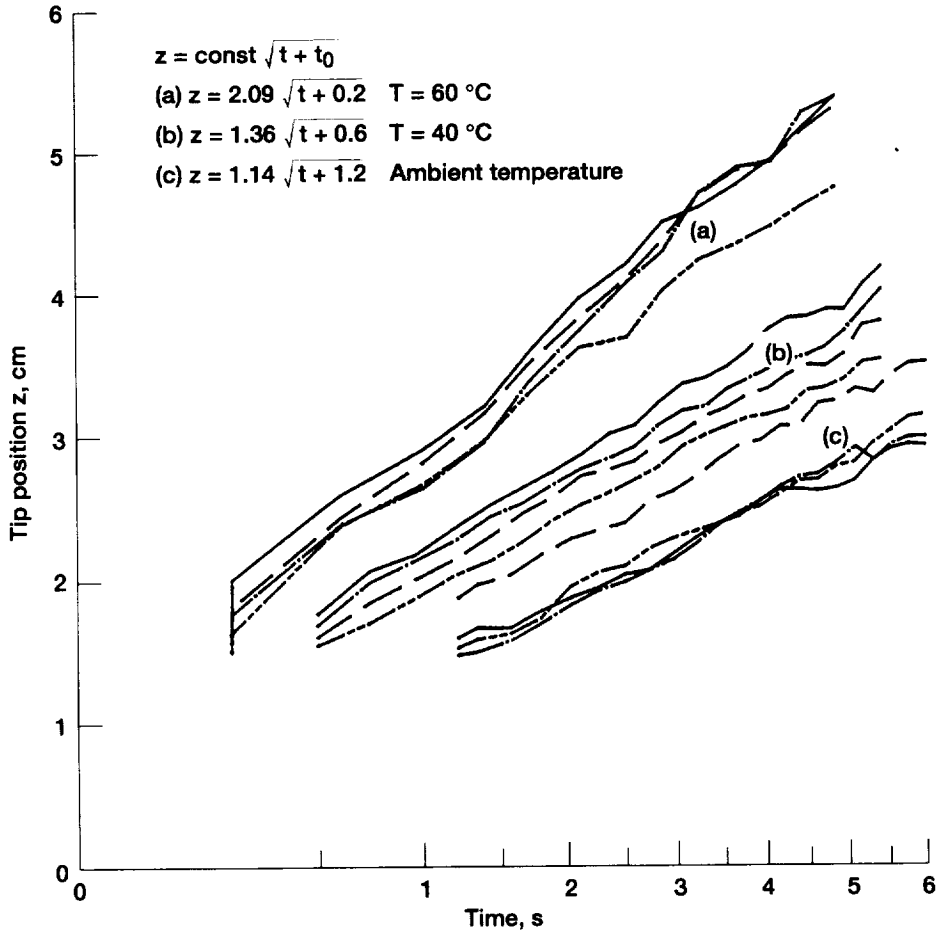

Figure 6.—Tip position versus $\sqrt{t}$ for drop tower tests. Represented by $z = C(t + t_0)^{1/2}$, the spreading coefficient C increases and the delay time t_0 decreases with increasing temperature.

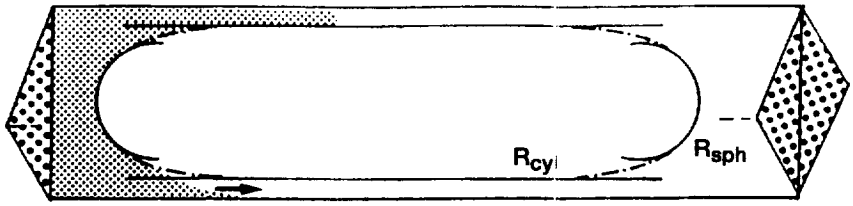

Equal curvature in wedges and cylinder ends: $R_{sph} = 2R_{cyl}$

Characteristic length of exponential adaptation: $R\sqrt{L_1}$

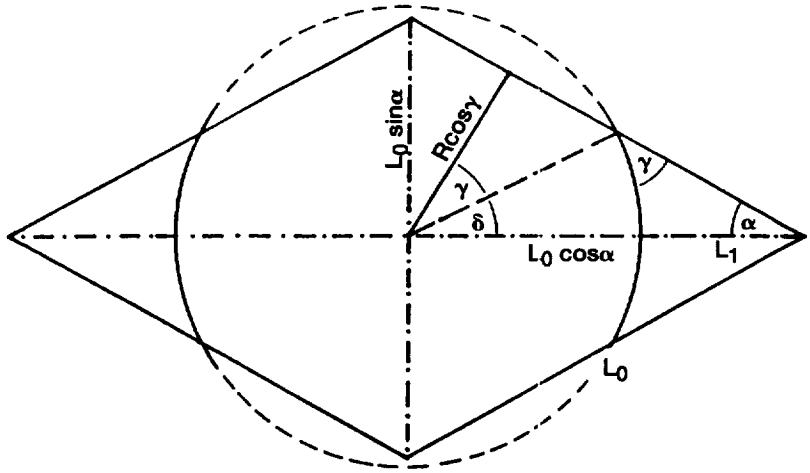

L_0 width of faces; $\delta = \pi/2 - \alpha - \gamma$

R = cylinder radius: $R\cos\gamma = L_0 \cos\alpha \sin\alpha$

Meniscus height: RL_1 where $L_1 = \cos\gamma/\sin\alpha - 1$

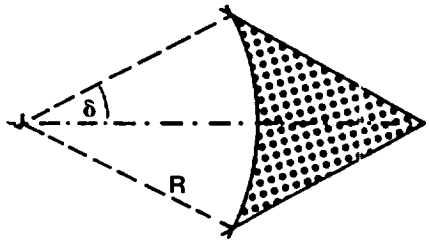

Cross-section area: $L_0 \cos\alpha\, R\sin\delta - R^2\delta = R^2 L_2$

where $L_2 = \cos\gamma/\sin\alpha \sin\delta - \delta \approx \delta(\cos\gamma/\sin\alpha - 1) \approx \delta^2 \cot\alpha$

Figure 7.—Sketch including notation for $\gamma \leq \pi/2 - \alpha$ analysis.

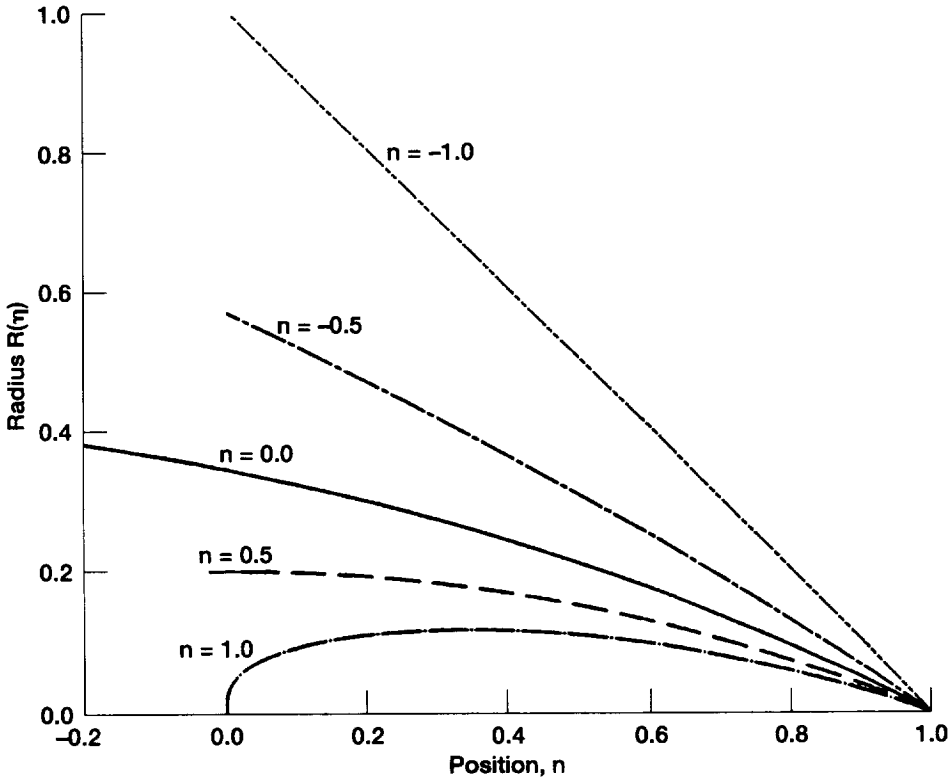

Figure 8.—The similarity solutions for fixed tip position for a variety of n's.

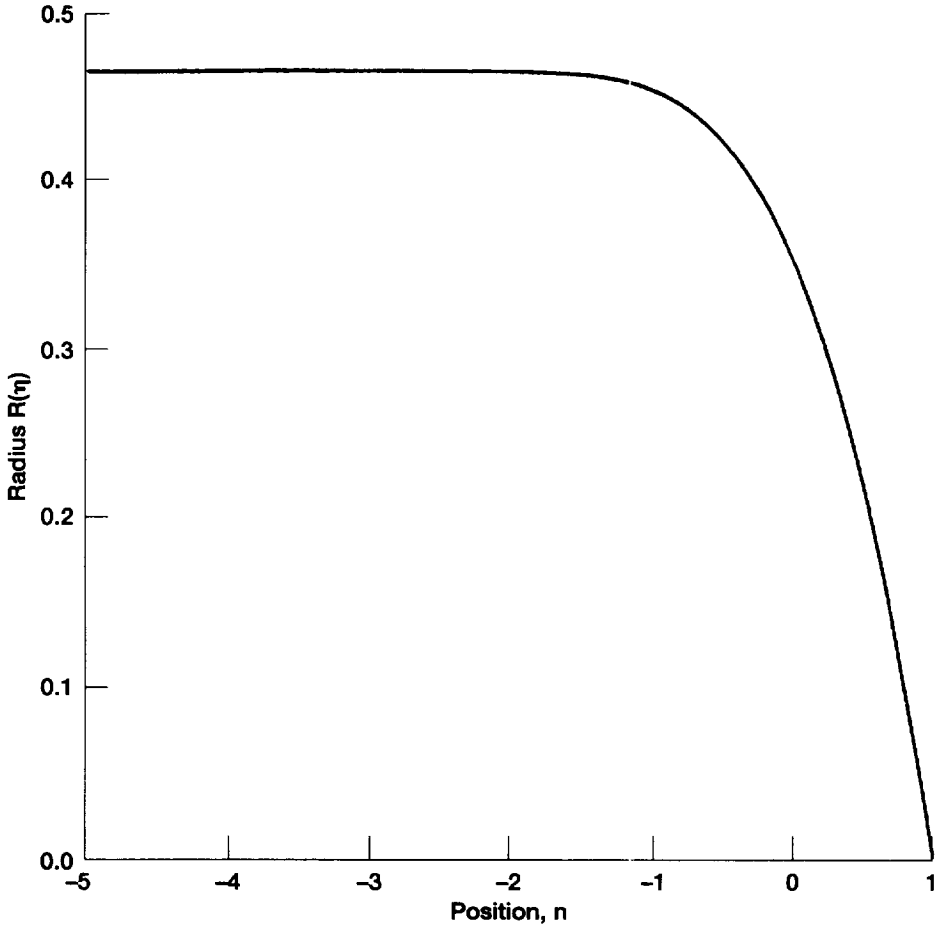

Figure 9.—The similarity solution rendering a constant meniscus height at minus infinity, n = 0.

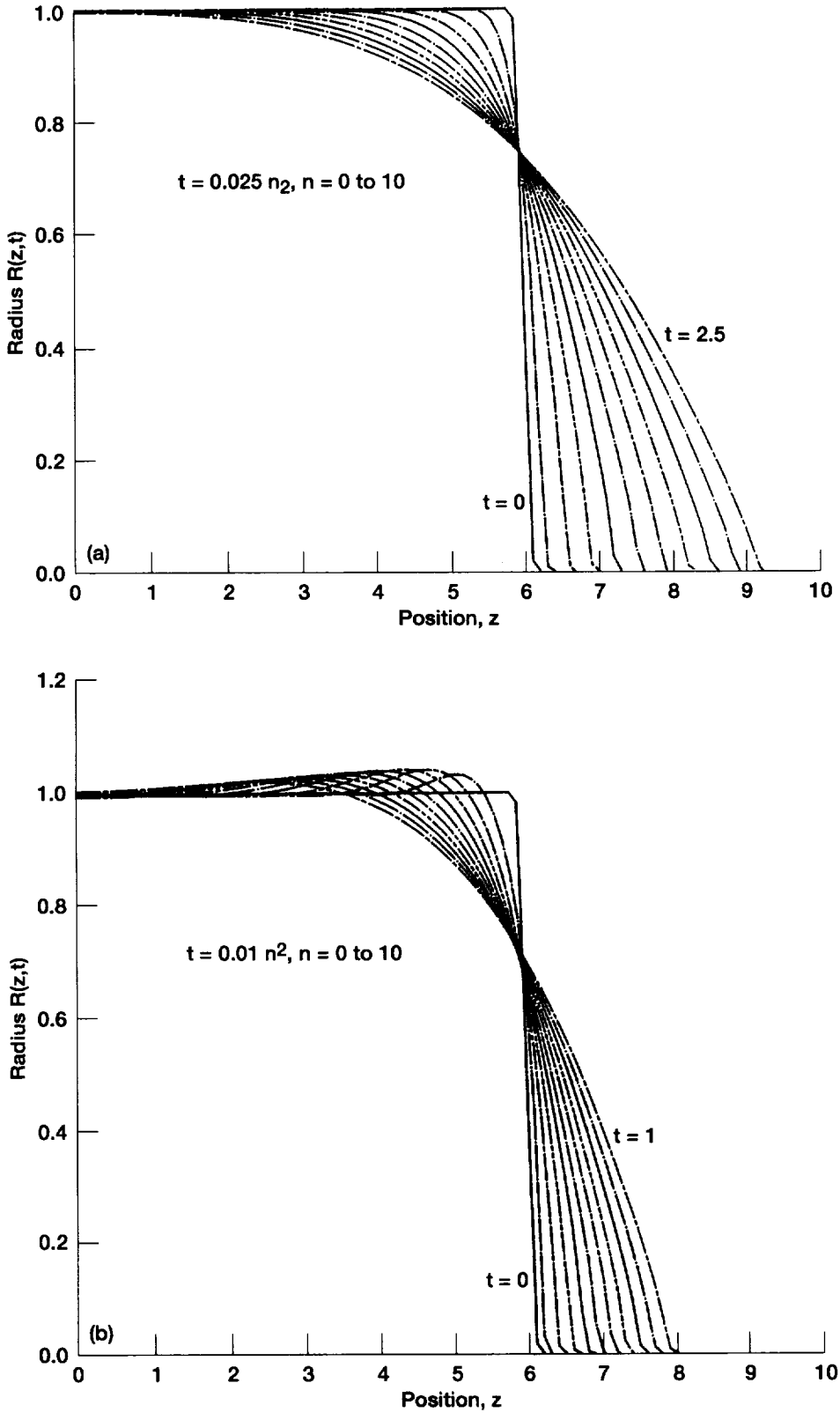

Figure 10.—Wetting of a wedge if the initial surface shape is a step function.
(a) Neglect of axial curvature (yields n = 0 solution). (b) Inclusion of axial curvature.
(c) With initial linear surface profile. (d) With an initial parabolic surface profile.

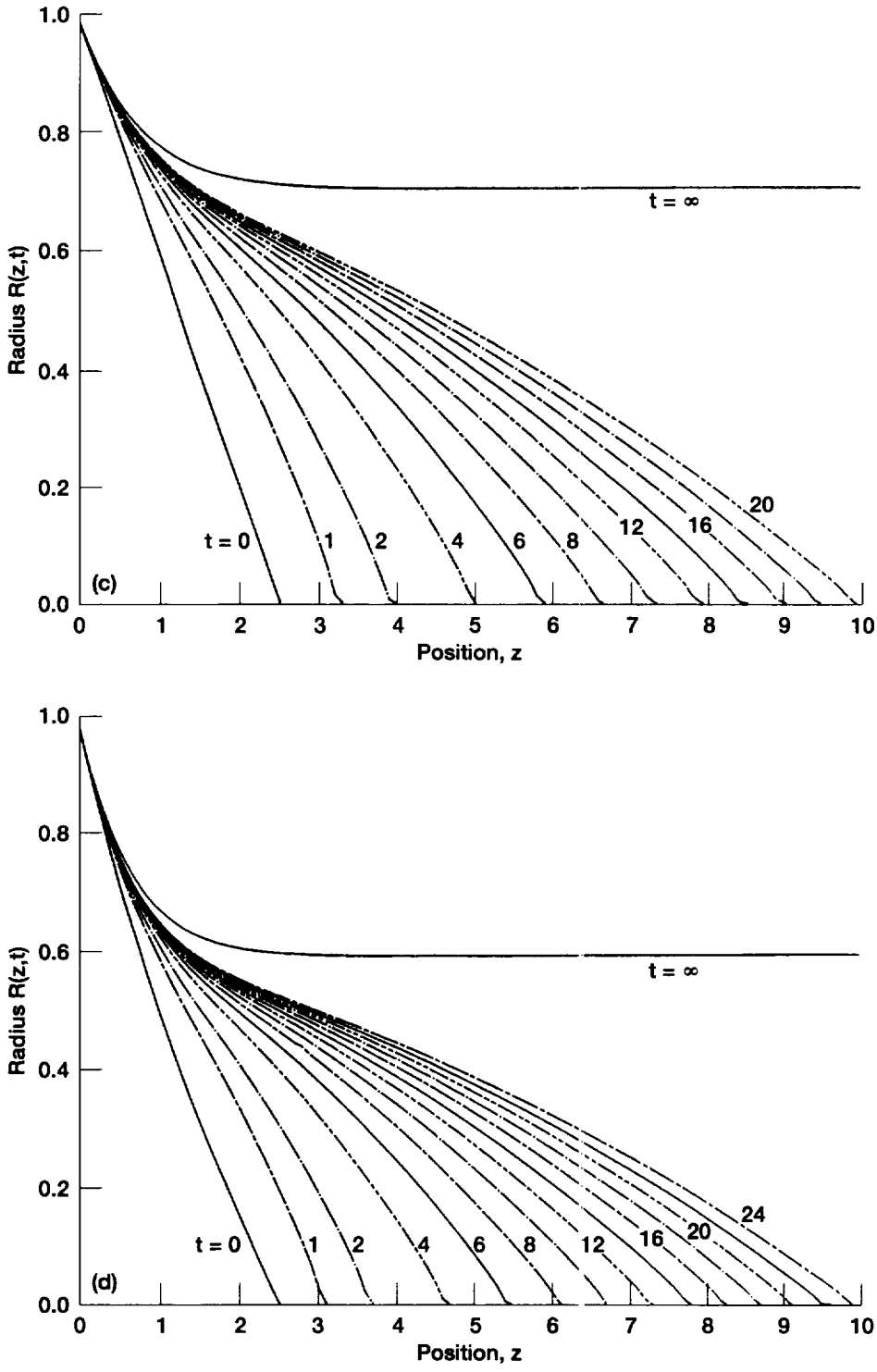

Figure 10.—Concluded. (c) With initial linear surface profile. (d) With an initial parabolic surface profile.

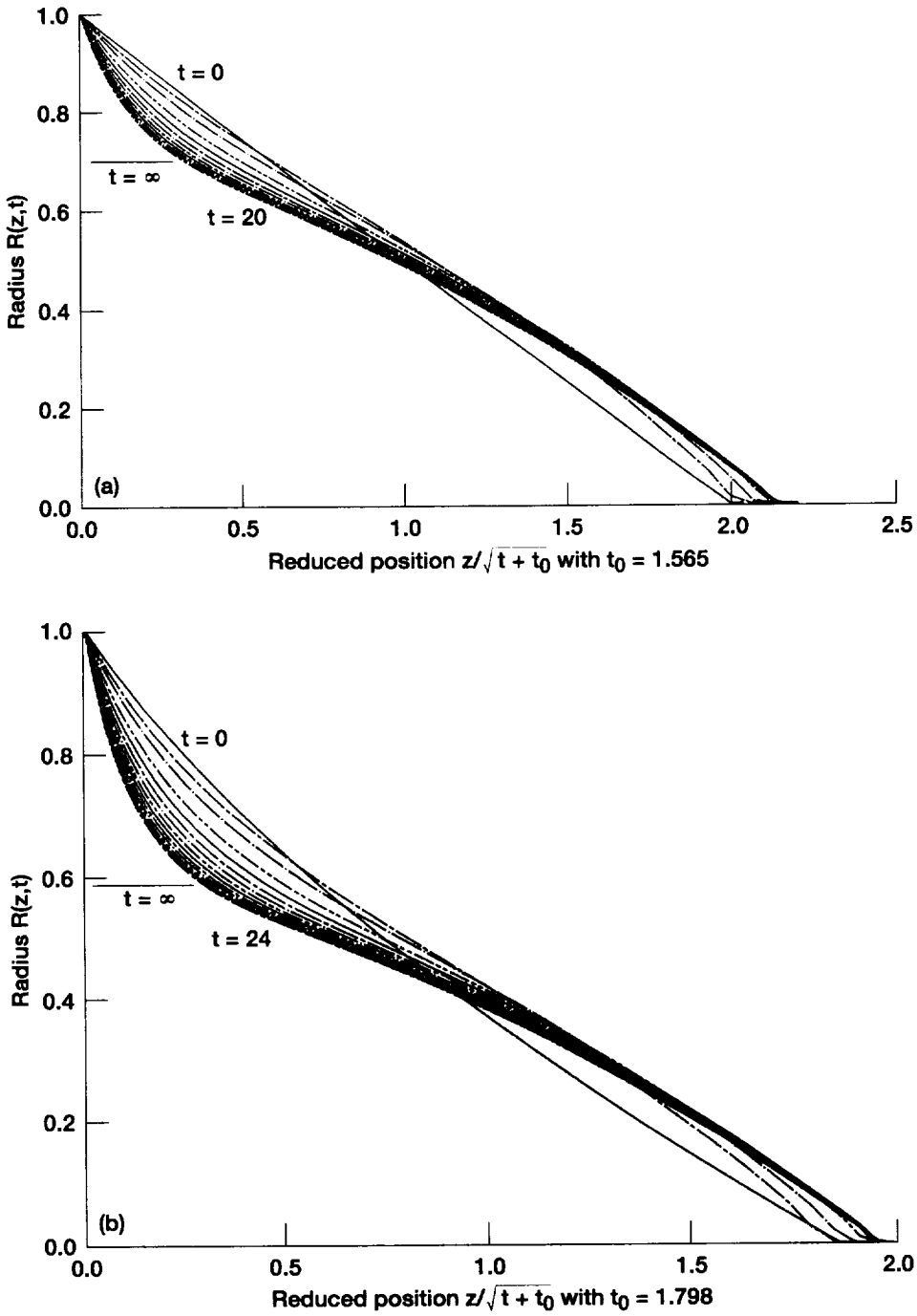

Figure 11.—The meniscus shapes shown in Fig. 10c, d versus the reduced position $z(t + t_0)^{-1/2}$. This demonstrates the eventual approach to the similarity of n = 0. (a) Linear initial profile. (b) Parabolic initial profile.

REPORT DOCUMENTATION PAGE

Form Approved
OMB No. 0704-0188

1. AGENCY USE ONLY (*Leave blank*)	2. REPORT DATE	3. REPORT TYPE AND DATES COVERED
	August 1998	Technical Memorandum

4. TITLE AND SUBTITLE

Dynamics of Liquids in Edges and Corners (DYLCO)
IML–2 Experiment for the BDPU

5. FUNDING NUMBERS

WU–962–24–00–00

6. AUTHOR(S)

D. Langbein and M. Weislogel

7. PERFORMING ORGANIZATION NAME(S) AND ADDRESS(ES)

National Aeronautics and Space Administration
Lewis Research Center
Cleveland, Ohio 44135–3191

8. PERFORMING ORGANIZATION REPORT NUMBER

E–11190

9. SPONSORING/MONITORING AGENCY NAME(S) AND ADDRESS(ES)

National Aeronautics and Space Administration
Washington, DC 20546–0001

10. SPONSORING/MONITORING AGENCY REPORT NUMBER

NASA TM—1998-207916

11. SUPPLEMENTARY NOTES

D. Langbein, ZARM, University of Bremen, Germany and M.M. Weislogel, NASA Lewis Research Center (presently with TDA Research, Inc., 12345 West 52nd Avenue, Wheat Ridge, Colorado 80033). Responsible person, M.M. Weislogel, organization code 6712, (303) 940–2320.

12a. DISTRIBUTION/AVAILABILITY STATEMENT

Unclassified - Unlimited
Subject Categories: 34, 18, and 28 Distribution: Nonstandard

This publication is available from the NASA Center for AeroSpace Information, (301) 621–0390.

12b. DISTRIBUTION CODE

13. ABSTRACT ***(Maximum 200 words)***

Knowledge of the behavior of fluids possessing free surfaces is important to many fluid systems, particularly in space, where the normally subtle effects of surface wettability play a more dramatic and often surprising role. DYLCO for the IML–2 mission was proposed as a simple experiment to probe the particular behavior of capillary surfaces in containers of irregular cross section. Temperature control was utilized to vary the fluid-solid contact angle, a questionable thermodynamic parameter of the system, small changes in which can dramatically influence the configuration, stability, and flow of a capillary surface. Container shapes, test fluid, and temperature ranges were selected for observing both local changes in interface curvature as well as a global change in fluid orientation due to a critical wetting phenomenon. The experiment hardware performed beyond what was expected and fluid interfaces could be readily digitized post flight to show the dependence of the interface curvature on temperature. For each of the containers tested surfaces were observed which did not satisfy the classic equations for the prediction of interface shape with constant contact angle boundary condition. This is explained by the presence of contact angle hysteresis arising from expansion and contraction of the liquid during the heating and cooling steps of the test procedure. More importantly, surfaces exceeding the critical surface curvature required for critical wetting were measured, yet no wetting was observed. These findings are indeed curious and pose key questions concerning the role of hysteresis for this critical wetting phenomena. The stability of such surfaces was determined numerically and it is shown that stability is enhance (reduced) when a surface is in its 'advancing' ('receding') state. The analysis shows complete instability as the critical wetting condition is reached. The case of ideal dynamic wetting is addressed analytically in detail with results of significant flow characteristics presented in closed form. The solutions indicate a $\sqrt{t}$ dependence of the capillary 'rise' rate which is corroborated by drop tower tests. The analysis clearly shows that infinite time is necessary for surfaces to reorient at the critical wetting transition.

14. SUBJECT TERMS	15. NUMBER OF PAGES
Wetting contact angle; Interior corner contact angle hysteresis; Microgravity	35
	16. PRICE CODE: A03

17. SECURITY CLASSIFICATION OF REPORT	18. SECURITY CLASSIFICATION OF THIS PAGE	19. SECURITY CLASSIFICATION OF ABSTRACT	20. LIMITATION OF ABSTRACT
Unclassified	Unclassified	Unclassified	